New perspectives into the rheology of earth suspensions modified with algae-derived biopolymers

Mojtaba Kohandelnia, Mahmoud Hayek, Kamal Bouarab, Ammar Yahia

Construction and Building Materials 503 (2025) 144523

Contents lists available at ScienceDirect

Construction and Building Materials

journal homepage: www.elsevier.com/locate/conbuildmat

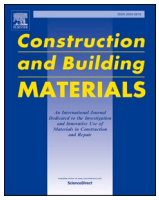

New perspectives into the rheology of earth suspensions modified with algae-derived biopolymers

Mojtaba Kohandelnia [a,*], Mahmoud Hayek [a,b,c], Kamal Bouarab [b], Ammar Yahia [a,d]

[a] Université de Sherbrooke, Department of Civil and Building Engineering, Sherbrooke, Québec, Canada
[b] Université de Sherbrooke, Department of biology, Sherbrooke, Québec, Canada
[c] LMGC, Univ Montpellier, IMT Mines Ales, CNRS, Ales, France
[d] Canadian University Dubai, City Walk, Dubai, United Arab Emirates

ARTICLE INFO

Keywords:
Algae
Biopolymer
Earth Suspension
Rheology
Viscosity-Modifying Agent (VMA)

ABSTRACT

Earthen materials provide a sustainable, low-carbon alternative for construction due to their natural abundance and minimal processing requirements. This study investigates the incorporation of algae-derived biopolymers to enhance the rheology and mechanical performance of cement-stabilized earth materials, aiming to improve construction efficiency while preserving environmental advantages. Three biopolymers extracted from red (carrageenan), brown (alginate), and green (ulvan) algae, each characterized by its principal polysaccharide, were incorporated into cement-stabilized earth suspensions to evaluate their effects on hydration kinetics (isothermal calorimetry), phase evolution (XRD), bleeding, pore solution chemistry (ICP-OES), rheology (visco-elastoplastic behavior), and compressive strength. The algae-based viscosity-modifying agents (VMAs) altered hydration process and improved suspension stability, with the degree of modification depending on the biochemical composition and pre-treatment of the biopolymers. The most significant hydration delay was observed with preheated brown algae, extending the induction period to approximately 88 h, while the highest 28-day compressive strength (4.8 MPa) was achieved with direct incorporation of biopolymer. SEM analyses revealed that algae-based biopolymers promoted a denser microstructure by refining the C-S-H gel, improving the interfacial transition zone (ITZ), reducing portlandite crystal size, and promoting the formation of biogenic calcite, collectively contributing to improved mechanical performance and durability.

1. Introduction

Cement is one of the most widely produced materials worldwide, yet its manufacture is responsible for approximately 8 % of global CO_2 emissions [1]. To mitigate its environmental footprint, the construction sector has increasingly adopted mitigation strategies such as the incorporation of supplementary cementitious materials (SCMs) and the optimization of mix designs, both aimed at enhancing sustainability, lowering emission, and improving structural durability [2–4]. Alongside these approaches, there is growing interest in earth-based construction materials as environmentally friendly alternatives with the potential to significantly reduce the ecological impact of the built environment. Traditional techniques such as wattle and daub, cob, adobe bricks, and rammed earth (RE) typically rely on clay and silt as binding agents, combined with sand and gravel as aggregates [5,6]. These materials are typically used in a dry state and require intensive compaction, as in compressed earth blocks, to achieve sufficient strength. Because of their abundance and local availability [7], earth-based materials offer several advantages, including low embodied energy, natural thermal regulation, improved indoor air quality, versatility, and aesthetic flexibility. They can also perform effectively with or without cement or lime stabilization, depending on the application [8–10]. Despite these benefits, their labor-intensive production, time-consuming construction process, and susceptibility to moisture-related degradation remain significant barriers to broader adoption.

Self-consolidating earth concrete (SCEC) offers a promising solution to the limitations of traditional earthen construction by combining the sustainability of earth-based materials with the fluidity and ease of placement characteristics of self-consolidating concrete (SCC) [6,11]. In contrast to traditional concrete, which relies heavily on cement, SCEC represents a significant advancement in eco-efficient construction materials, aligning with global strategies to lower the environmental

* Correspondence to: Department of Civil and Building Engineering, 2500 Bd de l'Université, Sherbrooke, QC J1K 2R1, Canada.
E-mail address: Mojtaba.Kohandelnia@usherbrooke.ca (M. Kohandelnia).

https://doi.org/10.1016/j.conbuildmat.2025.144523
Received 25 August 2025; Received in revised form 20 October 2025; Accepted 12 November 2025
Available online 17 November 2025

footprint of the building industry [12,13]. Conventional cement-stabilized earthen materials, typically containing 4–12 % cement by mass, are generally restricted to non-structural applications due to their low compressive strength, often below 2 MPa [14]. By contrast, SCEC achieves compressive strengths reaching up to 12 MPa at 28 days [15], while maintaining comparable or even superior hygrothermal performance [16].

The development of SCEC, however, poses significant mix design challenges. Its binder system composed of clay, silt, and cementitious materials, requires careful optimization of the paste phase. In particular, the dispersion of fine clay particles plays a critical role, as their high surface area and tendency to flocculate can severely hinder flowability, workability, and self-consolidation [17]. Soils employed in earth-based construction exhibit considerable variability in clay contents and mineral compositions, which provides flexibility in material selection but also poses significant challenges [18]. Clay minerals, characterized by their fine particle sizes and high specific surface areas (SSA), increase interparticle friction and consequently elevate both yield stress and plastic viscosity, factors that limit the flowability and workability of earth suspensions [19–22]. Beyond particle size, the shape and mineralogy of particles [7] further influence rheological behavior, often resulting in inconsistent performance across different soils. This complexity makes it difficult to predict the suitability of a given soil for SCEC without detailed characterization [23]. To ensure reliable performance, careful soil selection is required, with particular attention to clay content, mineral composition, and plasticity. Among key parameters, the Atterberg limits are especially useful for guiding SCEC mix design, as they correlate with both flow behavior and mechanical performance [15,17]. Ultimately, the plasticity index, largely governed by the quantity and fineness of the clay fraction, plays a decisive role in determining a soil's suitability for earth concrete applications [24].

Achieving sufficient early-age compressive strength for demolding remains one the key challenges in earthen construction. Several strategies have been explored to address this limitation. For instance, incorporating calcium sulfoaluminate cement (CSA) [6] or bio-based gelling agents such as alginate [25–28] has proven effective in accelerating strength development. The addition of SCMs can further contribute to early strength development [29], though selecting the appropriate blend of SCMs and fillers to simultaneously ensure optimal rheological behavior remains a complex task [30,31]. In the context of SCEC, the abundance of fine clay particles introduces additional challenges for flowability. Their type, quantity, and interaction with dispersing agents significantly influence fresh-state behavior, underscoring the role of rheology in governing both early workability and long-term performance of earthen materials [22,29,32]. Beyond chemical and admixture-based strategies, mechanical grinding and thermal activation have also been shown to enhance the reactivity of clay-rich soils, thus improving their bonding and contributing to higher strength and durability [33,34].

Recent studies have highlighted the potential of polysaccharide-based admixtures to enhance the mechanical and durability performance of clay and cementitious materials [35]. Brzyski and Gazda [36] demonstrated that methylcellulose addition (0.4 % of clay mass) significantly improved the compressive and flexural strength of clay mortars while reducing shrinkage and enhancing water resistance. Similarly, Brzyski [37] showed that gum arabic incorporation (1–3 %) increased strength by up to 170 % and reduced total porosity by 12 %, providing a pathway toward moisture-stable clay mortars. These findings confirm that biopolymer admixtures can balance strength, water resistance, and drying behavior in earthen materials. Complementary studies in cement-based systems have reported analogous trends. Losini et al. [38] and Trambitski et al. [39] reported that xanthan and guar gums modify hydration kinetics and improve workability without sacrificing mechanical strength. More Collectively, these studies highlight the potential of polysaccharides as eco-efficient rheological modifiers compatible with low-carbon construction materials. In parallel, alginate has gained attention for its ability to induce a liquid–solid transition through ionic cross-linking with Ca^{2+}, providing early cohesion in clay-based composites [40]. This mechanism, inspired by biopolymer gelation, offers promising routes for poured earth concretes, enhancing buildability and early stability. Despite these advances, most studies have focused on purified or extracted polysaccharides, leaving the direct use of unprocessed algae powders largely unexplored.

Globally, marine macroalgae represent an abundant renewable biomass, with more than 36 million tons harvested annually [41,42]. Brown, red, and green species contain distinct biopolymers such as alginate, carrageenan, and ulvan, that can modify hydration, improve particle cohesion, and stabilize suspensions through ionic complexation. For example, Autem et al. [43] demonstrated that parietal polysaccharides extracted from invasive Brittany seaweeds improved both mechanical and rheological properties of earth-based composites. Specifically, alginate from *Sargassum muticum* and carrageenan from *Solieria chordalis* enhanced compressive strength under both dry and humid conditions, while other polysaccharides significantly accelerated structural build-up, reducing processing times and improving 3D-printing suitability. Yet, despite this potential, the role of whole algae powders in cement-clay systems remains poorly documented.

Although plant-derived gums and purified biopolymers have been studied as eco-friendly admixtures, whole algae powders with complex biochemical compositions (polysaccharides, proteins, and minerals) [44] have not been systematically investigated in cement-stabilized earth suspensions. Therefore, understanding their influence on hydration kinetics, rheology, and microstructural development is essential for their effective use in sustainable construction.

Accordingly, this study aims to (1) evaluate the effects of red (carrageenan-rich), brown (alginate-rich), and green (ulvan-rich) algae powders on the hydration kinetics of kaolinite-rich cement-stabilized earth suspensions; (2) analyze their impact on pore-solution chemistry, rheology, and structural build-up; (3) investigate their influence on microstructure and compressive strength; and (4) assess the effect of pre-activation and direct addition methods to identify the most suitable incorporation approach for practical applications.The findings aim to support the design of optimized earth suspension formulations, thereby advancing and promoting the broader adoption of these eco-efficient, low-carbon materials in construction.

2. Experimental program

2.1. Materials and mixture proportions

In this study, the binder system for the earthen material consisted of high purity kaolinite clay and quartz silt, with general-use Portland cement incorporated as a stabilizing agent. All three components were incorporated in powder form in the earth suspension formulations. Their chemical compositions and physical characteristics are summarized in Table 1. To enhance workability, a polycarboxylate ether (PCE)-based high-range water-reducing admixture was employed, meeting the criteria of both Type A and Type F under ASTM C494 [45], with a

Table 1
Chemical composition and physical properties of the powders.

Chemical composition (% wt.)	**Cement**	**Kaolinite**	**Quartz silt**
CaO	62.50	0.10	0.01
SiO_2	19.30	46.10	99.02
Al_2O_3	4.80	38.10	0.64
Fe_2O_3	3.00	0.50	0.22
MgO	2.70	0.10	0.01
SO_3	4.10	0.04	-
Others	1.40	1.56	0.10
LOI*	2.20	13.50	-
Specific gravity	3.15	2.73	2.69
SSA (m^2/g)	0.30	14.8	0.20

density of 1.07 kg/L and solid fraction of 40 %. Four different biopolymeric admixtures were investigated: pure sodium alginate (MilliporeSigma, USA) and three dried, ground algae powders (SeaTech Bioproducts, USA), namely red algae (RA, rich in carrageenan), brown algae (BA, rich in alginate), and green algae (GA, rich in ulvan). The particle-size distribution (PSD) of the biopolymers and the mineral powders (cement, quartz silt, and kaolinite clay) is presented in Fig. 1.

The mix designs of the SCEC formulations are presented in Table 2. These mixtures were developed to reflect typical earth concrete compositions [15,17], incorporating a paste volume of 45 %, a volumetric cement-to-clay ratio of 0.6, a water-to-powder ratio (W/P) of 0.30, and a cement dosage of 90 kg/m^3 . A sand-to-total aggregate ratio of 0.9 was maintained across all mixtures. The selected paste volume and cement content were designed to achieve a balance between workability and compressive strength, following the recommendations of Kohandelnia et al. [15]. In line with previous findings [17], the W/P ratio of 0.30 was chosen for its ability to enhance compressive strength without substantially increasing the demand for the PCE-based water reducer, whose efficiency is primarily influenced by the fine fraction. The Atterberg limits of the earth binders, determined according to ASTM D4318 [46], yielded a liquid limit (LL) of 23 %, a plastic limit (PL) of 17 %, and a plasticity index (PI) of 6 %.

In this study, the paste fraction of the SCEC mixtures, referred to as earth suspensions, was prepared and analyzed. Sodium alginate was first dissolved in water at ambient temperature under continuous stirring for 30 min before mixing. Algae powders were incorporated using two methods: i) direct addition, in which the dry algae powder was dispersed in the mixing water and stirred until fully homogenized; and ii) pre-activation, following the procedure described in [44], where the algae powder was dispersed in water maintained at 40 °C, stirred continuously for 30 min followed by cooling to 23 °C without agitation for 2 h. The resulting solution was then used as the mixing water for preparing the earth suspensions. The resulting solutions were subsequently used as mixing water for preparing the earth suspensions.

The dosage of each biopolymer was expressed as a percentage of the mixing water mass. Sodium alginate was incorporated at 0.25 %, a value determined through preliminary flow-curve tests on cement pastes (water-to-cement ratio of 0.43) using a coaxial cylinder rheometer (Anton Paar MCR 302). In these tests, alginate dosages ranged from 0.05 % to 0.50 % of the water mass, and the resulting flow curves were fitted with the Bingham model to estimate yield stress and plastic viscosity parameters. The 0.25 % dosage was identified as the minimum effective concentration that produced a significant increase in plastic viscosity. The red and brown algae powders were each used at 1 %, while the green algae powder was incorporated at 2 %. These dosages were selected to achieve earth suspensions with fresh-state viscosities comparable to that of the 0.25 % alginate mixture, as determined by the same flow-curve testing protocol. Following mixing with the earth binders and cement, PCE was added to adjust workability and achieve a target mini-slump flow (MSF) of 280 ± 20 mm, as recommended to ensure adequate flowability of earth suspensions [17].

2.2. Test methods

All mixtures were prepared following ASTM C305 [47] using a planetary Hobart mixer. The MSF of the earth suspensions was assessed using the cone test [48] immediately after mixing and again 30 min after initial water-powder contact. The methodologies for calorimetry, X-ray diffraction (XRD), inductively coupled plasma (ICP) analysis, rheology, bleeding, mechanical testing, and scanning electron microscopy (SEM) are presented in this section.

2.2.1. Calorimetry and XRD

Hydration kinetics were monitored over 150 h using an isothermal TAM Air Calorimeter (TA Instruments, Sweden) maintained at 20 °C. Approximately 9.78 g of freshly mixed paste was sealed in glass ampoules immediately after mixing to prevent moisture loss. The heat flow was continuously recorded, and the results were normalized to the cement mass to determine the heat evolution rate (mW/g) and cumulative heat release (J/g). All measurements were performed in triplicate to ensure data reproducibility. After 28 days of curing at 23 °C and 100 % relative humidity, crystalline phases and structural modifications were characterized by XRD. Diffraction patterns were collected using a Panalytical X-Pert Pro MPD diffractometer with Cu Kα radiation (40 kV, 30 mA), scanned over a 2θ range of 5° to 70°, with a step size of 0.02° and a scan rate of 1°/min.

2.2.2. ICP

ICP analyses were conducted on the pore solution extracted from the forced bleeding tests at 0 and 30 min. The concentration of dissolved ions, including Ca^{2+}, K^{+}, Na^{+}, Mg^{2+}, Al^{3+}, and SO_4^{2-}, were quantified using an ICP spectrophotometer [49]. Immediately after extraction, the pore solutions were diluted at a ratio of 1:2500 with 2 % nitric acid to ensure accurate detection. Each sample was analyzed in duplicate to verify the reproductively of the measured ionic concentrations.

2.2.3. Rheology

Rheological properties were evaluated using an Anton Paar MCR 302 rheometer under controlled temperature conditions (23 ± 1 °C). Due to the presence of coarser silt particles in the powder fraction, measurements were performed with a parallel plate geometry and a fixed gap of 3 mm. This configuration was selected as a compromise between

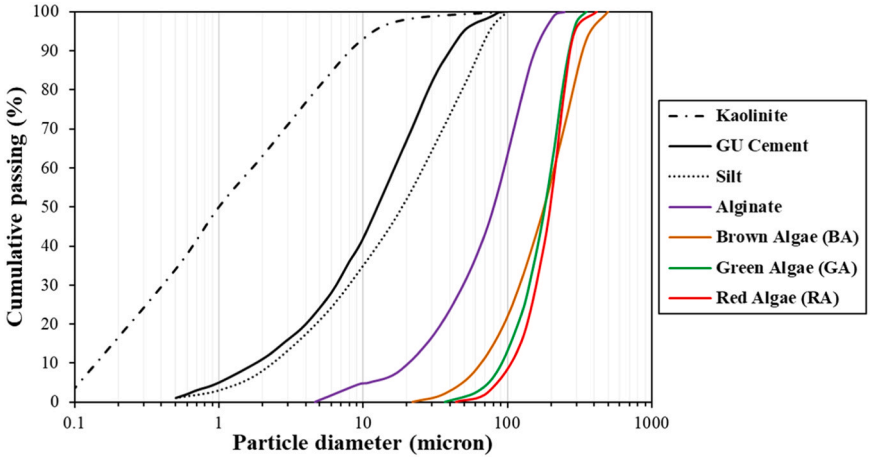

Fig. 1. Particle-size distribution of the investigated powders.

Table 2
Mixture proportions of the investigated SCEC mixtures.

Mix	Cement (kg/m^3)	Water (kg/m^3)	Clay (kg/m^3)	Silt (kg/m^3)	Sand (kg/m^3)	Gravel (kg/m^3)	Biopolymer (% of water)	W/P
Ref	90	203	130	458	1197	136	-	0.30
Alg	90	203	130	458	1197	136	Alginate (powder - 0.25 % of water)	0.30
RA-D	90	203	130	458	1197	136	Red algae (powder - 1 % of water)	0.30
RA−40	90	203	130	458	1197	136	Red algae (40 °C pre-activation)	0.30
BA-D	90	203	130	458	1197	136	Brown algae (powder - 1 % of water)	0.30
BA−40	90	203	130	458	1197	136	Brown algae (40 °C pre-activation)	0.30
GA-D	90	203	130	458	1197	136	Green algae (powder - 2 % of water)	0.30
GA−40	90	203	130	458	1197	136	Green algae (40 °C pre-activation)	0.30

providing sufficient sample volume for representative testing and minimizing normal force fluctuations associated with excessively thick samples. Similar gap settings have been adopted in rheological investigations of cementitious and earthen suspensions [22,34]. To minimize wall slip, the tested mixtures exhibited high intrinsic yield stress and strong particle interlocking, which inherently reduces slip at the plate interface. Moreover, no discontinuities or abrupt stress drops were observed during testing, further confirming negligible wall slip effects. The repeatability of the measurements, confirmed by triplicate tests with low variability, further indicates a consistent interaction between the sample and the plate surfaces.

The viscoplastic behavior of the paste mixtures was evaluated immediately after mixing and again after 30 min using a shear protocol consisting of a pre-shear phase at 150 s^{-1} for 120 s, followed by a gradual decrease to 1 s^{-1} over 105 s, as shown in Fig. 2a and recommended by [22]. The Bingham model ($\tau = \tau_0 + \mu_p \times \dot{\gamma}$) was applied to determine the rheological parameters, where τ is the shear stress, τ_0 the yield stress, μ_p the plastic viscosity and $\dot{\gamma}$ the shear rate. The Bingham model was selected as it provided the highest fit statistics across all mixtures, while Herschel-Bulkley fits provided negligible improvement ($\Delta R^2 < 0.02$) with flow index values close to unity, confirming quasi-linear (i.e. Bingham) behavior. Due to its simplicity, interpretability, and broad acceptance in rheological studies of stabilized earth-based suspensions [22,34], the Bingham model was retained.

The structural build-up of the earth suspensions was evaluated through the evolution of static yield stress over time at rest. Static yield stress was measured at successive intervals following mixing to monitor the evolution of the internal structure over time. The rate of increase in static yield stress, expressed A_{thix}, was used as a thixotropic index, providing a measure of the degree of structuration within the suspension [50–52]. Although this approach offers direct insight into structural evolution, it is strongly influenced by the shear history imparted during the rheological testing protocol.

A constant shear rate protocol was applied to evaluate the static yield stress of the mixtures, as illustrated in Fig. 2b. Each sample was first subjected to a pre-shear phase at 200 s^{-1} for 2 min to homogenize the

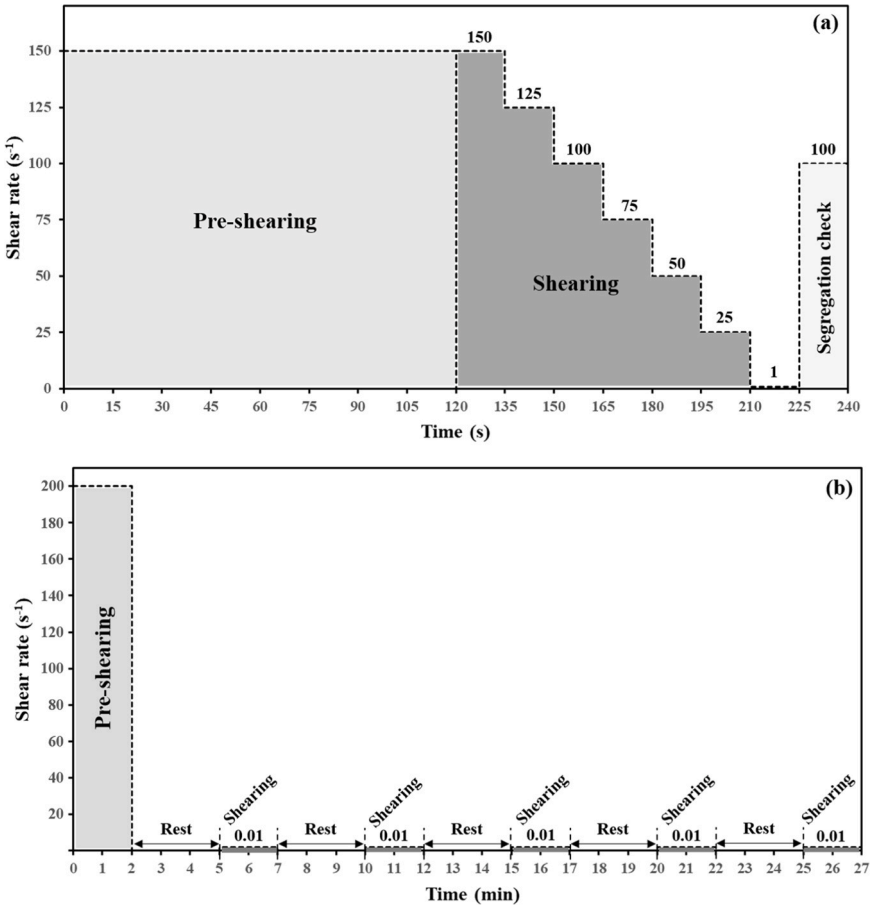

Fig. 2. Test protocol for (a) flow curve and (b) static yield stress measurements.

initial state and minimize variability due to sampling, as recommended in [53]. A constant shear rate of 0.01 s^{-1} was then maintained for 2 min, and the peak shear stress recorded during this phase was taken as the static yield stress. This procedure was repeated after rest intervals ranging from 5 to 20 min to capture the structural evolution over time. The increase in static yield stress with resting time, $\tau_{0\text{-}S}$ (t), was described using the equation $\tau_{0\text{-}S}$ (t) = $\tau_{0\text{-}S}$ (0) + t × A_{thix}, where A_{thix} denotes the thixotropic structuration rate, as proposed by Perrot et al. [50]. In addition, thixotropic behavior was further assessed using a hysteresis-loop shearing protocol. Following a pre-shear at 50 s^{-1} for 30 s and a 30-second rest at 0 s^{-1}, the shear rate was progressively increased from 0.1 s^{-1} to 150 s^{-1} over 90 s and then symmetrically decreased back to 0.1 s^{-1} over another 90-second, in line with the method proposed in [22]. In addition to the evolution of static yield stress ($A_{thix\text{-}static}$), the evolution of dynamic yield stress over the first 30 min was also assessed and is referred to as $A_{thix\text{-}dynamic}$ [34].

The viscoelastic behavior of the suspensions, particularly the critical shear strain ($\gamma_{critical}$) and storage modulus (G′), was assessed using the Small Amplitude Oscillatory Shear (SAOS) tests. To determine the critical shear strain, a strain sweep test was first performed by gradually increasing the strain from 0.0001 % to 100 % at a constant angular frequency of 10 rad/s. The critical shear strain was defined as the strain at which the storage modulus decreased to 90 % of of its maximum value (G'_{max}), following the procedure outlined in [53]. This value was then used in a time sweep test to monitor the evolution of G′ and loss modulus (G″) under non-destructive conditions. During the time sweep, a constant shear strain of 0.001 %, well below the critical threshold, was applied at 10 rad/s over a duration of 20 min, ensuring that the material response reflected elastic recovery behavior and preserved its solid-like structure without microstructural disruption [54]. Prior to both tests, the samples were pre-conditioned through a two-step shearing protocol: an initial rotational shear rate at 150 s^{-1}, followed by a brief Large Amplitude Oscillatory Shear (LAOS) phase at 6 % strain and 100 rad/s for 10 s, to ensure uniform dispersion withing the suspension [53].

By monitoring the evolution of G′ and G″, the phase angle (δ) was defined as $\tan^{-1}(G''/G')$, ranging from 0° to 90°. A phase angle of 0° corresponds to a purely elastic (solid-like) response with no lag between applied strain and resulting stress, whereas 90° represents a purely viscous (fluid-like) behavior [54]. Based on the smoothed profiles of G′ and δ over time, the kinetics of structural build-up in cement suspensions were characterized using two independent parameters. Firstly, the percolation time (t_{perc}), denotes the duration required for the formation of a continuous colloidal network and is identified at the point where δ stabilizes at its minimum value. Secondly, the rigidification rate (G_{rigid}), corresponds to the slope of the linear increase in G′ after percolation, reflecting the progressive reinforcement of mechanical integrity driven by cement hydration [51].

2.2.4. Bleeding

The bleeding resistance of earth suspensions was evaluated using a pressure filtration method [55,56], which measure the ability of fresh paste to retain its mixing water under sustained pressure. The setup consisted of a stainless-steel cylinder (44.5 mm in diameter, 140.0 mm in height) fitted with a Gelman-type membrane filter capable of retaining particles larger than 0.3 μm. For each test, 200 mL of fresh paste was introduced into the chamber and sealed, after which nitrogen gas was applied at a constant pressure of 80 psi for 10 min. The mass of water collected through the filter was recorded, and the forced bleeding after 10 min was expressed as a percentage of the initial mixing water in the sample. Tests were conducted at 0 and 30 min after mixing to assess the effect of structural build-up on water retention.

2.2.5. Mechanical properties and SEM

The mechanical and physicochemical properties of the investigated mixtures were comprehensively evaluated through standardized tests and advanced characterization techniques. Compressive strength was measured at 1, 7, and 28 days in accordance with ASTM C109 [57], using triplicate cube specimens (50 × 50 × 50 mm^3) to ensure statistical reliability. The samples were cured at 23 °C and 100 % relative humidity. Moreover, microstructure features and elemental composition of the 28-day cured samples were further examined by SEM coupled with energy dispersive X-ray spectroscopy (EDS), using a ThermoFisher Scientific Phenom XL G1 system.

3. Results and discussions

3.1. Calorimetric analysis

Fig. 3 and Table 3 present the heat evolution profiles obtained from isothermal calorimetry over 150 h for all investigated mixtures, highlighting the influence of algae-derived biopolymers on the hydration behavior of a kaolinite-rich concrete system. The reference mixture

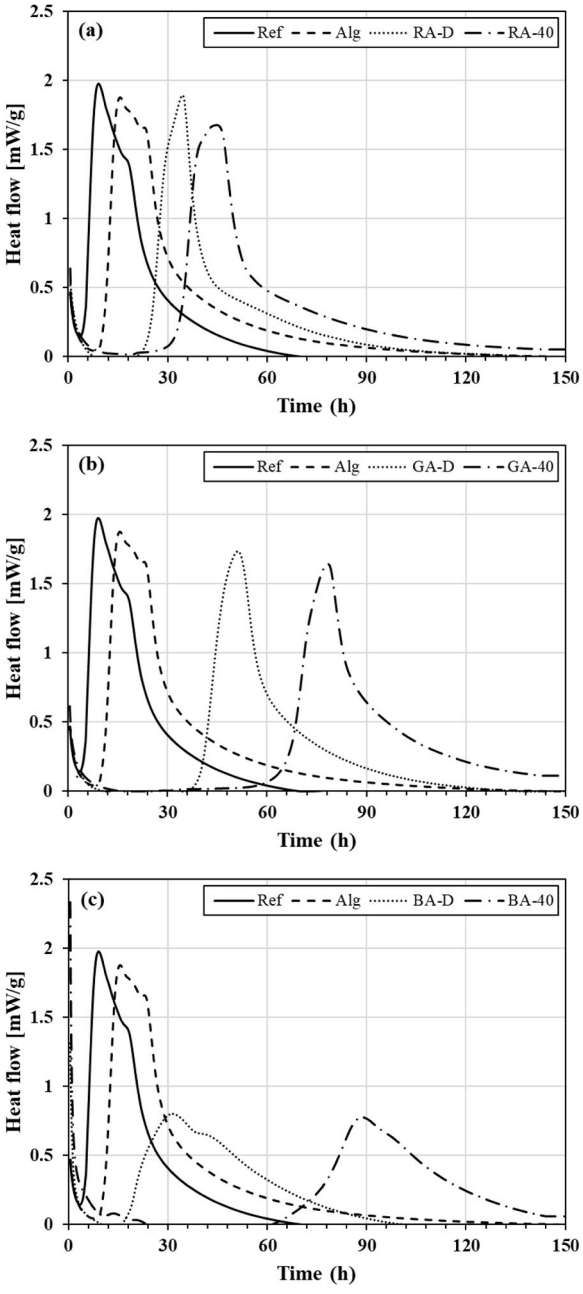

Fig. 3. Heat evolution profile of the investigated mixtures incorporating (a) red algae, (b) green algae, and (c) brown algae.

Table 3
Main, secondary peaks and cumulative heat release after 150 h observed in the investigated mixtures.

Mix	Main peak (mW/g)	Secondary peak (mW/g)	Time of primary peak (h)	Time of secondary peak (h)	Cumulative heat release after 150 h (J/g)
Ref	1.98	1.42	9.1	17.9	128.98
Alg	1.88	1.64	15.6	23.4	158.44
RA-D	1.89	-	33.4	-	132.95
RA−40	1.68	-	44.8	-	163.04
BA-D	0.80	0.65	31.5	41.4	107.66
BA−40	0.78	-	88.6	-	111.22
GA-D	1.74	-	51.2	-	133.15
GA−40	1.64	-	78.2	-	152.81

(Ref), without bio-based additive, exhibited two distinct exothermic peaks: the first at 9.1 h with a maximum intensity of 1.98 mW/g, and the second at 17.9 h with a lower intensity of 1.42 mW/g (Table 3). While dual-peak profiles are typically associated with cement hydration, in this context they more likely reflect the multi-stage reactivity of kaolinite in alkaline media [34]. The first peak can be attributed to alkali-induced activation of kaolinite, involving surface deprotonation, cation exchange (mainly with Ca^{2+} and Na^{+}), and partial dissolution of Al^{3+} and Si^{4+} from the clay layers, leading to the initial formation of calcium silicate hydrate (C-S-H) phases [58,59]. The second peak is associated with the precipitation of secondary products, such as calcium-alumino-silicate hydrates (C-A-S-H), likely resulting from pozzolanic reactions between the released aluminosilicate species and portlandite or dissolved alkalis. This two-stage hydration pattern is consistent with previous findings on calcined or natural kaolinite-based cementitious systems [34,60].

When pure alginate was used, the hydration kinetics were delayed, though the characteristic two-stage reactivity was preserved. The main exothermic peak shifted from 9.1 h (Ref) to 15.6 h, and a slight reduction in intensity from 1.98 to 1.88 mW/g (Table 3). A secondary peak was still observed, occurring at 23.5 h with a higher intensity (1.64 mW/g) compared to the reference (1.42 mW/g). These results indicate that alginate delays hydration but does not inhibit the multi-stage reactivity of the kaolinite-cement system. This retardation effect is likely due to the adsorption of alginate molecules onto kaolinite and cement particles, which creates a physical barrier limiting ion exchange and water penetration [61]. Furthermore, the carboxylate groups of alginate can chelate Ca^{2+} and Al^{3+} ions, delaying the nucleation and precipitation of hydrate phases [62,63]. Recent experimental and theoretical studies also suggest that alginate can chemically bonds with Ca^{2+}/Al^{3+} on kaolinite surfaces, forming ionic crosslinks that generate a network structure capable of trapping kaolinite particles in suspension and physically restricting their reactivity [64].

In contrast, the use of red and green algae, whether dried (-D) or preactivated (-40), caused both a stronger delay and a complete suppression of the secondary hydration peak (Figs. 3a and 3b). In all four cases, the main exothermic peak was significantly delayed, occurring at 33.4 h (RA-D), 44.9 h (RA-40), 51.2 h (GA-D), and 78.3 h (GA-40) (Table 3). This pronounced retardation highlights the strong inhibitory effects of both algal types, with GA-40 exhibiting the longest delay among all tested mixtures. The inhibition can be attributed to the nature and solubility of the bioactive polysaccharides released by the algae [65]. Red algae, rich in κ-carrageenan, contain high sulfate content and strong gelling capacity, enabling the formation of electrostatic complexes with Ca^{2+} and Al^{3+} and dense surface coatings on reactive mineral particles [56]. Green algae, in contrast, contain uronic-acid-rich polysaccharides such as ulvan, which exhibit strong Ca^{2+}-chelating ability and high-water retention capacity [66,67]. Thermal pre-activation at 40 °C further amplified these effects by promoting the release of both high-molecular-weight polysaccharide and soluble low-molecular-weight fractions, thereby increasing ionic binding and viscous resistance in the pore solution [44] The resulting higher viscosity reduces ionic mobility, slows dissolution and precipitation processes, and ultimately contributes to the overall retardation of hydration. The complete suppression of the secondary hydration peak suggests that red and green algae not only delayed kaolinite activation but also inhibited its subsequent reactivity. This behavior likely results from a combination of chemical mechanisms (ion complexation and surface adsorption) and physical mechanism (diffusion resistance and protective film formation) [56,57,64,65,66]. As noted by Peschard et al. [65], the interaction between polysaccharide and cementitious system is inherently complex, depending on the polysaccharide's structure, solubility, and the mineralogical/chemical composition of the mixture. For example, their study showed that dextrinization starch exerted stronger inhibition than native starch due to its higher solubility [65]. Similarly, in this study, the combined chemical and physical effects of algal polysaccharides appear to be responsible for the total suppression of kaolinite's secondary hydration peak.

In the case of brown algae, the heat evolution exhibited a distinct profile marked by both a pronounced delay and a strong inhibition of hydration kinetics (Fig. 3c). The primary exothermic peak occurred at 31.6 h with a significantly reduced intensity of 0.80 mW/g. This effect was even further amplified in BA-40, where the peak was further delayed to 88.7 h and the intensity decreased to 0.78 mW/g (Table 3). Although alginate is the principal bioactive polysaccharide in brown algae, the hydration behavior of BA-D and BA-40 did not replicate that of the pure alginate-based mixture. This difference suggests that other constituents of the brown algae matrix, such as insoluble fibers, polyphenolic compounds, proteins, and minerals, exert a stronger influence on hydration than alginate alone [68]. The delay observed for BA-D and BA-40 can be partly explained by mechanisms similar to those proposed for green and red algae (ion complexation, surface adsorption, and increased viscosity). However, the origin of the stronger inhibition remains less straightforward. One possibility is that brown algae release higher concentrations of chelating agents, leading to more efficient sequestration of Ca^{2+} and thereby suppressing not only early hydration but also the formation of secondary products.

Overall, algae-derived VMAs affected the hydration process differently depending on their type and treatment. Pure alginate moderately delayed hydration without altering the characteristic two-stage reactivity of kaolinite. In contrast, red and green algae caused substantial delays and completely suppressed the secondary peak, thereby inhibiting pozzolanic reactions. Brown algae produced pronounced retardation and reduced the cumulative heat release, suggesting that constituents other than alginate, such as fibers, polyphenols, proteins, and minerals play a dominant role in inhibiting hydration. These findings highlight the complex interplay between chemical mechanisms (ion complexation, adsorption) and physical process (diffusion, viscosity) governing biopolymer–mineral interactions.

In addition to these mechanisms, differences in the ionic strength of the pore solution may also contribute to the observed hydration behavior. The dissolution of soluble salts naturally present in the algae (e.g., Na^{+}, K^{+}, Cl^{-}, and SO_4^{2-}), can modify the chemical environment of the suspension by altering ion activities and saturation states [69,70]. Such changes may influence the dissolution rate of reactive phases and the precipitation kinetics of hydrates, thereby contributing to the delayed exothermic response. Although this hypothesis was not quantitatively assessed in the present study, it provides a complementary explanation that should be explored in future work through systematic monitoring of ionic concentrations coupled with calorimetric analysis.

3.2. *ICP insights into ion release and consumption during initial hydration*

The ICP analyses performed at 0 and 30 min provide key insights into the early-stage ionic dynamics that govern hydration kinetics in earth suspensions modified with biopolymers [71]. These results (Fig. 4)

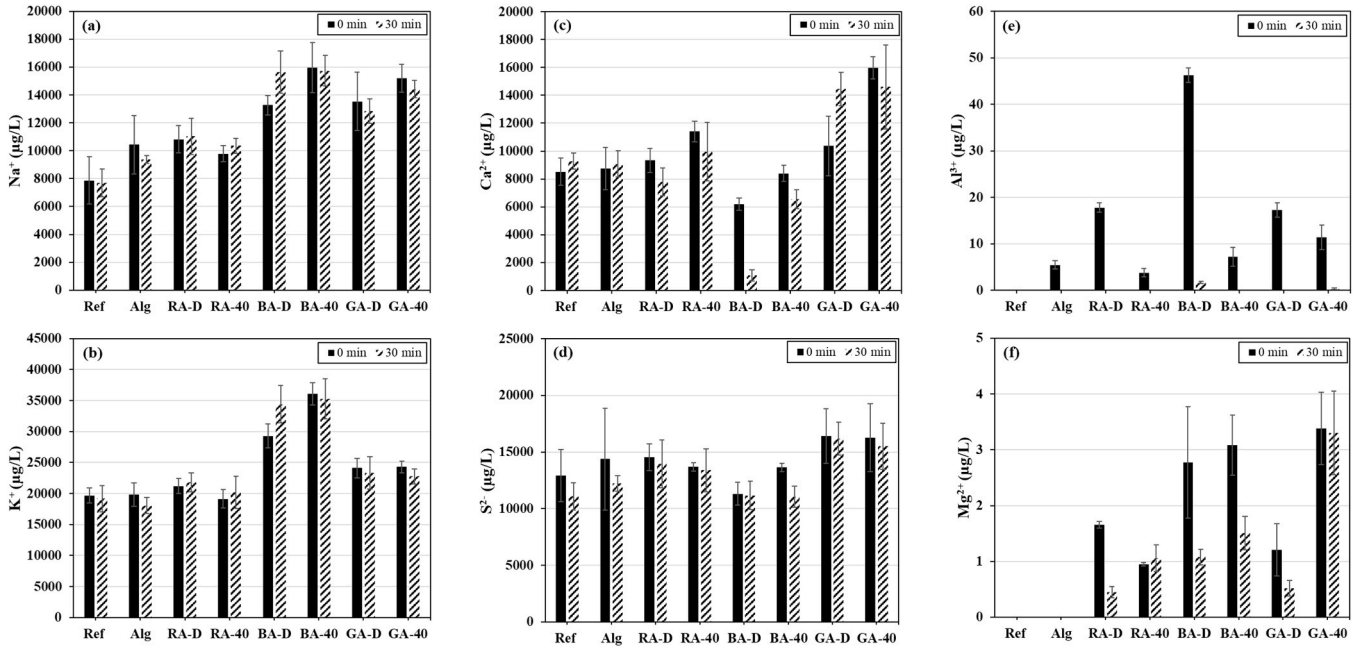

Fig. 4. ICP analysis of the investigated earth suspensions: (a) Na^+, (b) K^+, (c) Ca^{2+}, (d) S^{2-}, (e) Al^{3+}, (f) Mg^{2+}.

reveal two sequential phases. At 0 min, the ionic profile reflects the initial enrichment arising from cement dissolution and the contribution of the biopolymer additives. By 30 min, the results show the early-stage ionic consumption, complexation, or immobilization related to mineral reactions and/or biopolymer interactions.

Upon contact with water, partial dissolution of Portland cement releases Na^+, K^+, Ca^{2+}, and SO_4^{2-} into the pore solution. The early presence of Na^+ (Fig. 4a) and K^+ (Fig. 4b) is mainly attributed to the dissolution of alkali-sulfate phases [72], whereas Ca^{2+} (Fig. 4c) and SO_4^{2-} (Fig. 4d) originate from the dissolution of gypsum ($CaSO_4$ 2 H_2O) and anhydrite ($CaSO_4$) and are subsequently involved in the early formation of portlandite ($Ca(OH)_2$) [73]. Notably, Al^{3+} (Fig. 4e) was not detected at 0 min in the reference mixture, consistent with previous studies reporting aluminum concentrations typically below 1 mmol/L during the first stages of cement hydration [72,74]. In contrast, kaolinite dissolution under alkaline conditions is known to release Al^{3+} through partial depolymerization and leaching of aluminosilicate layers. The absence of Al^{3+} in the reference mixture therefore indicate that the detected ions at this stage derive exclusively from cement, with no measurable contribution from kaolinite [75].

Relative to the reference mixture, sodium alginate (pure biopolymer) had little influence on the concentrations of K^+ (Fig. 4b), Ca^{2+} (Fig. 4c), and SO_4^{2-} (Fig. 4d) in the pore solution at 0 min. However, it caused a significant increase in Na^+ (Fig. 4a) and the appearance of detectable amount of Al^{3+}. The high Na^+ concentration is attributed to the intrinsic sodium content of alginate and its solubility in water. The presence of Al^{3+} likely reflects early interactions between alginate and cement, particularly through perturbation of tricalcium aluminate (C_3A) dissolution and/or the inhibition of ettringite nucleation. Comparable effects were reported by Caruso et al. [71], who showed that polycarboxylate-based superplasticizers can promote transient Al^{3+} release by interfering with C_3A reactivity. Altogether, these results suggest that sodium alginate interacts engages in early chemical interactions with cement phases, likely through adsorption onto particle surfaces and coordination with multivalent cations [76], consistent with the hydration delay observed in calorimetry for the alginate-modified mix.

Unlike the sodium alginate mixture, the use of red (RA), green (GA), and brown (BA) algae powders, whether in dried (-D) or preactivated (-40), induced much stronger modification in the ionic composition of the pore solution at 0 min. All algae-containing mixtures exhibited higher concentrations of Na^+, K^+, Ca^{2+}, and SO_4^{2-}, along with detectable levels of Mg^{2+} and Al^{3+}, compared to the reference. These differences are primarily attributed to the marine origin and complex composition of algal biomass, which contains soluble salts, trace metals, and bioactive polysaccharides [63,77–80]. Upon mixing with water, these components are rapidly released into the pore solution, while pre-activation at 40 °C further promotes leaching by enhancing the solubility of both ionic and organic fractions [44].

For example, GA-D and GA-40 released up to 15 208 µg/L of Na^+, 24 283 µg/L of K^+, and 15 970 µg/L of Ca^{2+}, with SO_4^{2-} concentrations exceeding 15 000 µg/L. The detection Al^{3+} across all algae types may reflect early interactions between algal biopolymers and C_3A, similar to alginate, while the simultaneous presence of Mg^{2+}, absent in both the reference and alginate mixtures, points to an additional biogenic source likely originating from mineral-organic complexes in the algal matrix. These findings support the view that whole algal powders influence cement hydration not only through their polymer chemistry but also via their inherent ionic load, particularly in pre-activated (-40) forms that intensify the release of soluble fractions. Such early ionic enrichments are critical, as they modify the chemical environment of the mix from the very first moments after water addition. As demonstrated by Peschard et al. [65] and Lothenbach & Winnefeld [72], variations in early ion concentration can influence particle charge distribution, nucleation thresholds, and competitive sorption, all key factors in hydration [71]. In this context, algae-derived biopolymers act as both rheology modifiers and ionic modulators, potentially contributing to the retardation observed in calorimetry through coupled chemical and electrostatic pathways.

After 30 min of hydration, the ionic concentration in the pore solution of the Ref mixture remained relatively stable, indicating that kaolinite dissolution had not occurred even at this stage. However, the alginate containing mixture maintained elevated Na^+ levels, consistent with the continuous dissolution of sodium alginate, while no Al^{3+} was detected. This transient behavior of Al^{3+} likely reflects its immobilization, either through complexation with the carboxylate group of alginate [81] or by adsorption on cement and kaolinite particles [82]. In addition, the absence of Ca^{2+} depletion, despite the known chelating ability

of alginate [83], suggests that Ca^{2+} complexation is limited under the present conditions during the first 30 min. Instead, alginate appears to form surface-adsorbed layers or weak complexes that modify cement-clay interactions without significantly depleting ions from solution [84]. This interpretation supports the view that the hydration delay observed in the alginate system arises mainly from colloidal and adsorption-driven mechanisms, rather than from ionic consumption or the inhibition of cement dissolution.

In the case of seaweeds, all mixtures containing raw algae powders, regardless of algal type (red, green, or brown) or pre-treatment (dried -D, preactivated −40), showed a reduction in Ca^{2+} and Al^{3+} concentrations compared to their initial (0 min) values. In most cases, Al^{3+} dropped to undetectable levels, indicating a strong sequestration of trivalent cations by algae-derived polysaccharides. This behavior is consistent with the ability of sulfated and uronic-acid biopolymers (e.g., κ-carrageenan in red algae, ulvan in green algae, alginate in brown algae) to form stable hydrogels with multivalent cations [85–87] or to promote ion adsorption onto cement and clay particle surfaces [71]. The behavior of Ca^{2+} varied among algae types. In RA and GA systems, Ca^{2+} levels decreased moderately but remained above those of the reference mixture. In contrast, both BA-D and BA-40 displayed Ca^{2+} concentrations lower than the reference after 30 min, suggesting stronger calcium binding or precipitation in the brown algae systems. This finding is consistent with the hydration kinetics, where significant retardation was observed only in BA systems. Such Ca^{2+} depletion is critical, as it can hinder the early formation of ettringite and C-S-H, thereby intensifying hydration inhibition [88].

Further investigation is required to establish a systematic comparison among the different algae types and to clarify the differences observed between pure biopolymer (sodium alginate) and its raw source (brown algae). Overall, the 30-minute ICP results indicate that whole algae powders act both as early ion donors (at 0 min) and as efficient chelators for Ca^{2+}, Al^{3+}, and Mg^{2+}, with brown algae exhibiting the strongest calcium sequestration relative to the reference. This dual ionic role, combined with the adsorption of algae-derived biopolymers to cement and kaolinite particles, provides a mechanistic explanation for the pronounced hydration retardation and suppression of the secondary calorimetric peak observed in RA, GA, and BA systems. Future investigations should include ICP measurements performed around the main hydration peaks to establish a more direct correlation between ion exchange, hydration reactions, and the evolution of mechanical and rheological properties, thereby providing a deeper understanding of ion exchange dynamics throughout the hydration process.

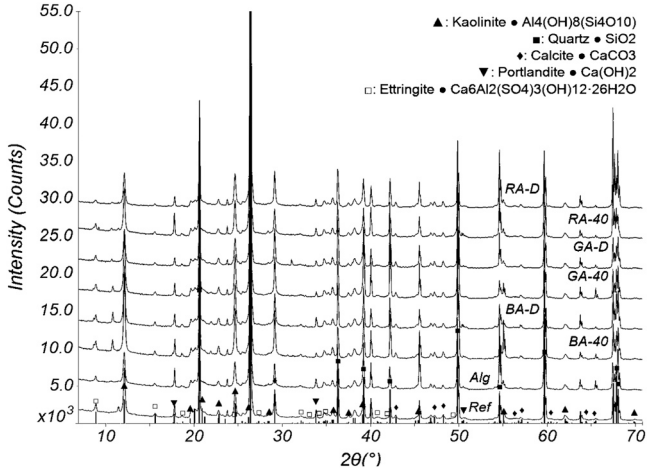

Fig. 5. XRD pattern of the investigated mixtures with and without algae-derived biopolymers at 28 days.

3.3. XRD analysis

Fig. 5 presents the XRD patterns of mixture with and without algae-derived biopolymers after 28 days of curing. The main crystalline phases detected in all samples were kaolinite, quartz, calcite, and ettringite. Incorporation of algae-derived biopolymers did not introduce new crystalline phases; however, it noticeably modified the relative peak intensities. These variations suggest that polysaccharide, mineral interactions can affect the dissolution of kaolinite and cement phases, after precipitation kinetics, and influence the extent of hydration product formation.

In the case of kaolinite, characteristic peaks at 12°, 20°, 24°, 39° and 46° 2θ are clearly visible in the reference mixture, with moderate intensity. This reflects the partial dissolution of kaolinite and its interaction with the alkaline pore solution and cement hydration products, as previously reported for raw kaolinite in blended systems [34,89–91]. After 28 days of curing, the presence of these peaks indicates that a fraction of kaolinite remained unreacted under the present conditions [89]. However, all algae-containing mixtures exhibit an increase in kaolinite peaks intensities relative to the reference, suggesting a reduced degree of kaolinite dissolution and transformation during early hydration. This effect is most pronounced in the pre-activated algae systems, particularly GA-40 and BA-40, and to a lesser extent in RA-D and RA-40. The observed trend can be attributed to the adsorption of algae-derived polysaccharides on kaolinite surfaces, which inhibit their dissolution and subsequent pozzolanic-type reactions with cement hydration products. As a result, a larger fraction of kaolinite remains crystalline for longer periods, delaying its conversion into secondary C-A-S-H phases. These findings are consistent with the study of Elert et al. [92], who demonstrated that organic matter can passivate clay mineral surfaces, significantly reducing their dissolution rates under highly alkaline conditions. The authors attributed this effect to the preferential adsorption of organic compounds at reactive sites on the clay surface, particularly at kaolinite edges, which restricts the access of the alkaline solution to dissolution-active sites. This passivation mechanism accounts for the slower dissolution of kaolinite observed in the algae-containing mixtures, where polysaccharides play a role analogous to naturally occurring organic matter in hindering mineral reactivity. This trend is further supported by calorimetry results, which revealed a marked delay in hydration and suppression of the secondary exothermic peak. The effect was most significant for BA-40 and GA-40, while RA-D and RA-40 exhibited shorter delays, consistent with the observed differences in kaolinite dissolution.

In the case of calcite, characteristic peaks at 29°, 43°, 47°, 48°, 53° and 66° 2θ are present in all mixtures. However, their intensities are higher in algae-containing mixtures, with the most pronounced increases observed in BA-D, BA-40, and GA-40. This enhancement can be attributed to the marine origin of the algal biomass, which naturally contains biogenic calcium carbonate, typically in the form of calcite or aragonite [93,94]. The incorporation of these mineral-rich powders thus directly increases the crystalline calcite content of the hardened matrix. While calcite may contribute as a fine filler and provide additional nucleation sites for C-S-H formation, in these systems its role remains secondary compared to the dominant chemical interactions between algae-derived polysaccharides and cement-clay particles, which primarily govern the hydration kinetics and microstructural evolution.

For portlandite and ettringite, the main diffraction peaks are located at 18°, 34° 2θ (portlandite) 8° and 16° 2θ (ettringite), and are detected in all mixtures. In the reference mixture, their intensities are consistent with the normal progression of cement hydration [95,96]. The presence of portlandite at 28 days indicates that its consumption through pozzolanic reactions with kaolinite or carbonation remains limited under the curing conditions applied. In mixtures containing algae-derived biopolymers, however, the peak intensities exhibited variable trends depending on the additive used. For instance, the portlandite peak at 18° 2θ is more intense than in the reference for Alg,

BA-40, and RA-40, but weaker in GA-D and comparable to the reference in other systems. A similar trend is observed for ettringite, with higher intensity in the alginate system and lower intensity in RA-D. These variations do not align consistently correlation with the trends revealed by ICP analyses or calorimetry, suggesting that the influence of algae-derived biopolymers on portlandite and ettringite formation or stability is complex. The discrepancies may arise from multiple concurrent factors, such as ion sequestration, modification in cement phase dissolution rates, and shifts in the timing of secondary reactions. Further investigations are therefore required to elucidate the mechanisms by which these bio-based additives modulate cement hydration products.

Therefore, the XRD results indicate that algae-derived biopolymers do not alter the nature of the main crystalline phases present after 28 days, but they do significantly modify their relative intensities. The most consistent effect is the preservation of kaolinite crystallinity, reflecting reduced dissolution and delayed pozzolanic reactions, particularly evident in BA-40 and GA-40 systems. These observations are consistent with calorimetry and ICP results, supporting the hypothesis that the primary inhibitory mechanism arises from the preferential adsorption of polysaccharides on kaolinite surfaces combined with the sequestration of multivalent cations, both of which modify the pore solution chemistry. In contrast, variations in portlandite and ettringite peak intensities were less systematic and did not always correlate directly with hydration kinetics, suggesting a more complex interplay of factors. Overall, the findings confirm that the inhibitory action of algae-derived biopolymers is mainly linked to their interaction with kaolinite and their capacity to modify the ionic environment, thereby delaying hydration and influencing microstructural evolution.

3.4. Workability and rheology

Table 4 summarizes the workability and rheological properties of the investigated earth suspensions. With a target MSF of 280 ± 20 mm, the reference, alginate, and RA-based mixtures achieved the desired MSF after PCE addition, whereas BA- and GA-modified suspensions reached saturation points at lower MSF values. This limitation is attributed to the strong adsorption of both biopolymers and PCE on mineral surfaces [76]. When the polysaccharide content is excessive, competitive adsorption dominates, diminishing the effectiveness and compatibility of the PCE. Biopolymer addition consistently increased PCE dosage requirements compared to the reference mixture (0.21 % of powders). Among the tested biopolymers, alginate required the lowest PCE demand, while RA-D and RA-40 required slightly higher amounts (0.28 % and 0.27 %, respectively). The higher water demand of alginate systems is attributed to hydrogel formation through cross-linking reactions, which absorb water during mixing [97]. While these hydrogels release part of the of the encapsulated water during setting, improving internal curing [98,99], they also generate macropores, potentially reducing density, compactness, and compressive strength. Overall, biopolymers significantly altered the fresh-state behavior of earth suspensions by modifying water and PCE demand. Their dual role, as both water absorbers and potential internal curing agents, suggest a complex balance between advantages and drawbacks, requiring further rheological investigation to elucidate the biopolymer's effects on rheology of earth suspensions.

3.4.1. Yield stress and plastic viscosity

Fig. 6 illustrates the relationship between static yield stress, dynamic yield stress, and plastic viscosity of the fresh mixtures immediately after mixing. The variability across the three repetitions is indicated by the error bars. Static yield stress followed the same trend as dynamic yield stress, with consistently higher values, in agreement with those reported in [34]. The reference mixture exhibited the lowest rheological parameters, with plastic viscosity, dynamic yield stress, and static yield stress of 0.52 Pa·s, 10.4 Pa, and 12.4 Pa, respectively.

Among the mixtures achieving the target MSF, alginate induced the

Table 4
Workability and rheological properties of the investigated earth suspensions.

Mixture	PCE demand	MSF (mm)		MSF loss (%)	Bingham model				$A_{thix\text{-}dynamic}$ (Pa/min)	$\gamma_{critical}$ (%)	$G'_{20\ min}$ (kPa)	t_{perc} (sec)	G_{rigid} (Pa/s)	Static yield stress (Pa)		$A_{thix\text{-}static}$ (Pa/min)	Hysteresis thixotropy (Pa/s)
		0 min	30 min		0 min		30 min							0 min	20 min		
					τ_0 (Pa)	μ (Pa.s)	τ_0 (Pa)	μ (Pa.s)									
Ref	0.21	270	230	14.8	10.4	0.52	21.2	14.8	14.8	0.011	8.5	350	17.8	12.4	45.9	1.68	−83.5
Alg	0.24	260	225	13.5	29.6	1.25	39.6	13.5	13.5	0.025	10.5	400	12.1	30.6	63.1	1.62	443.2
RA-D	0.28	260	195	25.0	19.4	1.11	41.1	25.0	25.0	0.018	52.9	500	56.4	22.4	71.6	2.46	1453.1
RA−40	0.27	270	200	25.9	14.3	0.94	35.5	25.9	25.9	0.018	33.7	500	33.9	17.2	58.7	2.08	1713.5
BA-D	0.29	230	165	28.3	31.6	1.55	50.3	28.3	28.3	0.030	15.3	450	17.9	33.7	73.9	2.01	947.3
BA−40	0.28	235	160	31.9	28.6	1.00	40.5	31.9	31.9	0.027	17.8	450	19.3	31.5	70.1	1.93	450.3
GA-D	0.27	225	200	11.1	18.5	1.18	39.3	11.1	11.1	0.022	21.8	500	22.1	20.3	61.1	2.04	811.8
GA−40	0.42	150	130	13.3	48.1	0.84	76.2	13.3	13.3	0.017	103.2	550	84.2	53.9	104.9	2.55	6852.4

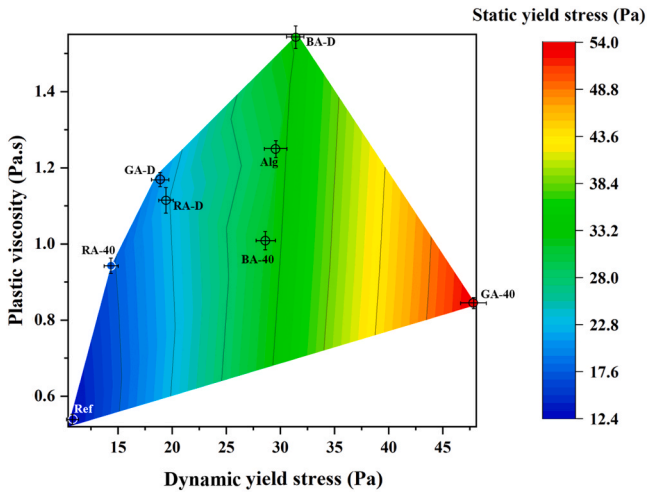

Fig. 6. Static yield stress as a function of Bingham yield stress and plastic viscosity.

highest plastic viscosity and yield stress values. Sodium alginate, derived from the cell walls of brown marine algae, is a water-soluble polysaccharide that undergoes a liquid-to-gel transition in aqueous media. This transition allows alginate chains to entangle and form a three-dimensional network, increasing flow resistance and yield stress [61, 100]. Its strong water-retention capacity further contributes to higher viscosity [56]. For other seaweed-based biopolymers, the elevated yield stress is likely associated with enhanced interparticle interactions and matrix densification, while the rise in viscosity may be attributed to gelation mechanism that reduce the amount of free water available in the suspension [101].

When comparing pre-activating at 40 °C with direct biopolymer addition, the pre-activated samples consistently exhibited lower viscosity values. Interestingly, this trend reversed in the absence of PCE, indicating that direct incorporation of biopolymers in the presence of PCE promotes stronger gel-like behavior by reducing the amount of free water within the matrix. Excluding the GA-40 mixture, which exhibited poor flowability due to polymer oversaturation, yield stress analysis revealed that RA-40 and BA-40 mixtures exhibited lower values than their direct-addition counterparts (RA-D and BA-D). The reduced yield stress in the pre-activated biopolymer systems can be attributed to the biopolymer's ability to suppress flocculation and agglomeration of kaolinite particles. This effect likely arises from the extended, partially folded configuration of polymer chains, which enhances network flexibility and facilitates alignment under shear. Previous studies [61] similarly reported that kaolinite–alginate suspensions exhibit lower flow resistance compared to unmodified kaolinite systems. In contrast, when biopolymers are directly incorporated in the presence PCE, stronger interparticle interactions result in higher yield stress.

The BA-D mixture exhibited the highest plastic viscosity and yield stress among all tested mixtures, a behavior directly attributed to its pore solution chemistry. ICP analysis revealed that BA-D contained the highest concentration of Al^{3+}, along with elevated levels of Na^{+}, K^{+}, and Mg^{2+}. Trivalent Al^{3+} ions are particularly effective in promoting strong interparticle attractions, acting as powerful double-layer compressors and form multiple coordination bonds with negatively charged sites on clay or silicate surfaces, thereby generating dense, space-spanning flocculated networks. Such enhanced aggregation increases both the force needed to initiate flow (yield stress) and the internal friction between moving flocs (plastic viscosity).

The elevated Na^{+} and K^{+} concentrations further contribute to double-layer compression by increasing the ionic strength of the pore solution, while Mg^{2+} contributes additional divalent bridging between particle surfaces, reinforcing the structural network. In BA–D, the synergistic presence of high-valency Al^{3+} and the substantial presence of Na^{+}, K^{+}, and Mg^{2+} produces a compact, interconnected microstructure characterized by strong particle–particle bonds. This explains the exceptionally high plastic viscosity and yield stress measured in this mixture.

3.4.2. Viscoelastic behavior

The relationship between percolation time, storage modulus after 20 min ($G'_{20\ min}$), and critical shear strain is illustrated in Fig. 7. Immediately following shear disruption, all mixtures exhibited near-zero G′ values and phase angle δ values exceeding 45°, reflecting minimal structural integrity and a predominantly liquid-like response. With increasing rest time, G′ progressively increased, indicating the gradual formation and stiffening of a particulate network. Concurrently, δ decreased and eventually stabilized, indicating a rheological transition from a fluid-like to a more solid-like state. Notably, previous studies have shown that δ is largely independent of hydration kinetics [51], supporting its relevance as a reliable descriptor of early-age physical structuration.

The results showed the lowest values of t_{perc}, $G'_{20\ min}$, and $\gamma_{critical}$ as 350 s, 8.5 kPa, and 0.011 %, respectively, suggesting that although the network forms rapidly, it remains weak due to limited cohesive interactions among flocs. In contrast, the incorporation of biopolymers increased both t_{perc} and $G'_{20\ min}$, reflecting slower network development but enhanced structural cohesion. The highest storage modulus was observed for RA and GA suspensions, with pre-activated samples showing even higher values. Among the biopolymer-based mixtures, the evolution of storage modulus for GA-40 and Alg, representing the highest and lowest values respectively, is illustrated in Fig. 8. This behavior can be attributed to reduced interparticle spacing and elevated solid content, which intensify particle–particle interactions and explain the significantly higher storage modulus [102]. However, the resulting dense and highly connected network also becomes more susceptible to disruption, as it serves as an efficient medium for stress transmission. Consequently, even small deformations can propagate through the structure, promoting particle rearrangement and leading to an earlier deviation from linear viscoelastic behavior [103]. This effect correlates with the elevated Ca^{2+} concentrations detected in the pore solution of RA and GA. Calcium ions facilitate ionic crosslinking between negatively charged sites, promoting rapid network formation while reducing electrostatic repulsion. The outcome is a stronger and more elastic microstructure, which accounts for the enhanced storage modulus observed in these mixtures.

As for the critical shear strain, earth suspensions inherently undergo

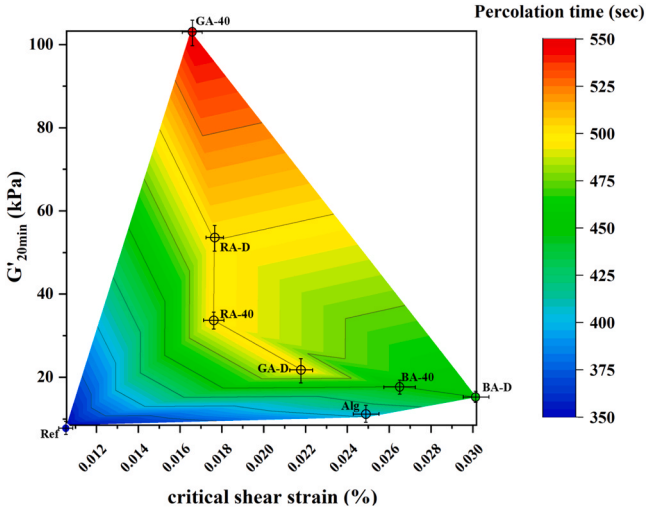

Fig. 7. Percolation time as a function of storage modulus and critical shear strain.

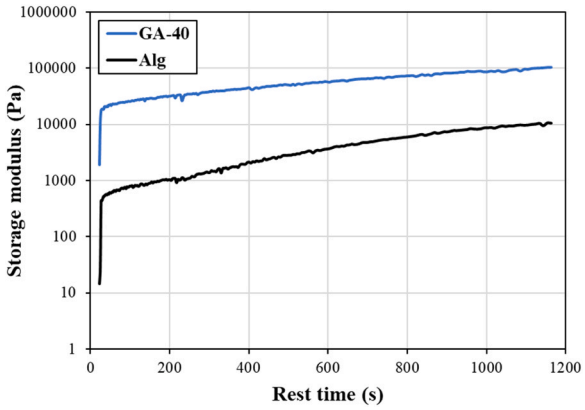

Fig. 8. Evolution of storage modulus over time for GA-40 and Alg mixtures.

particle flocculation, primarily driven by van der Waals attractions, which promotes the formation of a three-dimensional network structure [104]. This interconnected network enables the propagation of applied deformation throughout the suspension, resulting in the relatively low critical shear strain observed in the reference mixture. The introduction of biopolymer, however, alters this behavior. The BA-modified suspension exhibited the highest $\gamma_{critical}$ value (0.03 %), reflecting enhanced resistance to deformation before network breakdown. The variation among different biopolymers stems from the balance between electrostatic stabilization and polymer chain entanglement. In GA and RA suspensions, polymer overlapping progressively outweighs electrostatic contributions, leading to an increase in the plateau modulus but a corresponding reduction in $\gamma_{critical}$. Here, the electrostatic stabilization imparted by the polymers suppresses flocculation, disrupting the particle-driven network while simultaneously enhancing strain independence. As polymer chains overlap and entangle [105], the system transitions into a regime dominated by a three-dimensional polymer network, which governs its structural and mechanical response.

The elevated Al^{3+} concentration in the pore solution of the BA-D suspension strongly influences its microstructure by promoting ionic crosslinking and compressing the electrical double layer surrounding the particles. This results in the formation of a more rigid and interconnected particle network, capable of sustaining greater deformation before yielding, thereby increasing the critical shear strain. Furthermore, the relatively high concentrations of Na^{+}, K^{+}, and Mg^{2+} contribute to the overall ionic strength, which reduces electrostatic repulsion and facilitates stronger particle aggregation. Together, these ionic interactions foster the development of a robust internal structure that resists shear-induced breakdown up to higher strain levels, accounting for the maximum critical shear strain in BA-D.

3.4.3. Build-up

Fig. 9 illustrates the relationship between static and dynamic structural build-up indices, rigidification rate, and hysteresis thixotropy. Interestingly, alginate-modified suspensions exhibited slightly lower G_{rigid} and build-up indices compared to the reference mixture. This observation contrasts with the findings of Perrot et al. [28], who reported a marked acceleration in structural build-up when sodium alginate was used to stabilize earth mixtures with cement, relative to the unstabilized formulations. The present results indicate that, in cement-stabilized earth suspensions, the interaction between alginate and PCE does not significantly alter the structural build-up kinetics. Similar behavior was reported by Maierdan et al. [61] for kaolinite–alginate suspensions, where the flexible, well-dispersed microstructure facilitated smoother flow initiation with minimal structural collapse, thereby reducing thixotropy. However, as can be observed in Fig. 9b and Table 4, the alginate-modified mixture exhibited a thixotropic response, whereas the reference mixture was the only formulation displaying

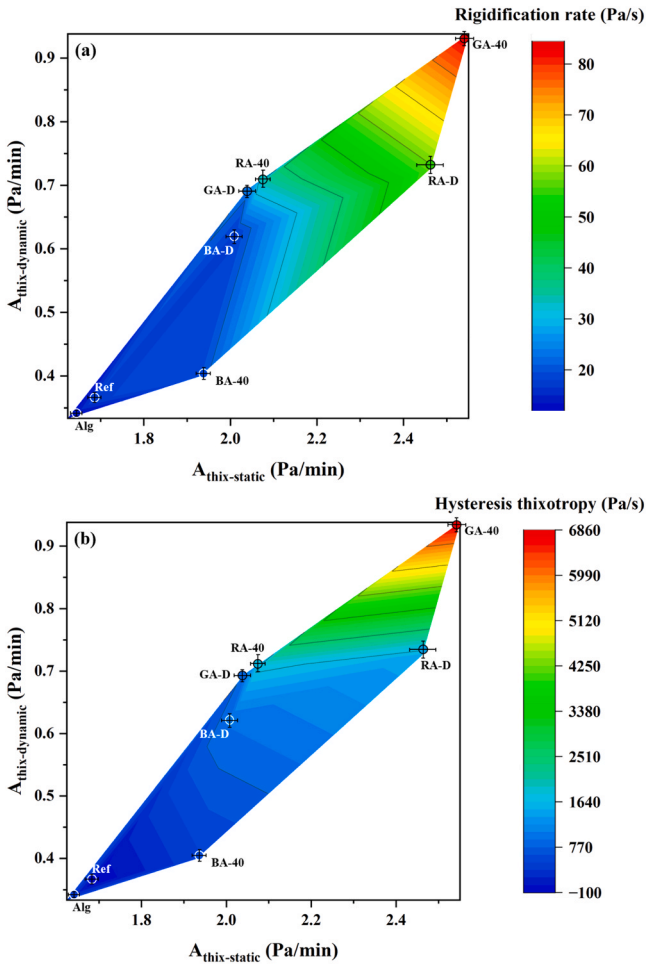

Fig. 9. Static and dynamic build-up indices as a function of (a) rigidificatin rate and (b) hysteresis thixotropy.

rheopectic behavior [22]. Among the biopolymers, the increasing hysteresis thixotropy closely followed the trends in rigidification rates, with GA-40 and RA mixtures showing the highest values.

Similar to the storage modulus results, GA and RA biopolymers produced the highest G_{rigid} and build-up indices. Earth suspensions with higher storage modulus values exhibited faster structural recovery over time, consistent with the finding of Maierdan et al. [61]. The significant build-up observed for Ulva polysaccharides aligns with results reported in [43], which demonstrated that Ulva effectively accelerate the structural consolidation of earth-based formulations. This behavior suggests that these biopolymers reduce interparticle spacing and increase local particle density, enhancing the probability of particle-particle interactions. Such densification promotes more rapid structural build-up, while polymer-particle associations further modify the network, leading to distinct interaction mechanisms among biopolymers.

ICP analysis of the pore solution revealed that GA and RA mixtures contained the highest concentrations of Ca^{2+} among all formulations. These elevated Ca^{2+} strongly influence the suspension microstructure through ionic crosslinking and double-layer compression. In systems with negatively charged particle surfaces or anionic polymeric additives, Ca^{2+} forms ionic bridges between adjacent particles or polymer chains, rapidly producing a percolated network at rest. At the same time, reduced electrostatic repulsion allows closer particle approach and enhances van der Waals attractions, accelerating flocculation [106]. These Ca^{2+}-mediated interactions not only promote faster structural build-up, reflected in higher rigidification rates, but also sustain a rigid network at rest that remains reversible under shear, consistent with the pronounced

thixotropic response observed in GA and RA. The correlation between pore solution Ca^{2+} concentration and rheological behavior thus demonstrates that Ca^{2+}-induced flocculation and bridging are the primary drivers of both accelerated rigidification and enhanced thixotropy in these systems.

3.5. Resistance to forced bleeding

Fig. 10 shows the forced bleeding measurements for earth suspensions with and without algae-derived biopolymers, measured immediately after mixing (0 min) and after a 30 min resting period. The reference mixture (Ref) exhibited the highest bleeding values, with 10.7 % at 0 min and 10.2 % at 30 min, reflecting the high availability of free water in the absence of biopolymers. Under applied pressure, this free water, unbonded within the microstructure or chemically bound to cement-kaolinite phases, can readily expelled from the suspension. However, all biopolymer-containing systems, whether with pure sodium alginate or raw algae powders, showed a significant reduction in bleeding compared to the reference. This trend is consistent with the literature, where biopolymers are reported to reduce bleeding in a dose-dependent manner by increasing viscosity, yield stress, and particle network cohesion, thereby limiting water migration under static or dynamic conditions [56,107–112]. Sodium alginate reduced bleeding to 7.9 % (0 min) and 7.3 % (30 min), consistent with its ability to form hydrated polymer networks that physically immobilize free water [113,114]. Raw algae powders produced variable effects depending on algal type and pre-treatment. BA systems (BA-D and BA-40) exhibited the lowest bleeding values (7.1–7.33 % at 0 min, 6.5–7.1 % at 30 min), in line with ICP results indicating strong Ca^{2+} sequestration suggesting the formation of highly crosslinked hydrogel networks that effectively immobilize water. RA systems (RA-D and RA-40) reduced bleeding to 7.3–7.9 %, attributed to the gelling ability of κ-carrageenan in the presence of multivalent cations [44,56]. GA systems also showed reduced bleeding (7.3–7.6 %), consistent with ulvan gel network formation under the prevailing ionic environment [115,116]. For all mixtures, both with and without biopolymer, bleeding decreased between 0 min and 30 min, indicating progressive structuration and hydration of the suspension during the resting period.

Therefore, the forced bleeding results clearly demonstrate that algae-derived biopolymers enhance the fresh-state stability of earth suspensions by limiting water migration under pressure. The reduction in bleeding can be attributed to two complementary mechanisms: i) physical immobilization of water by long-chain polysaccharides, which increases viscosity, yield stress, and network cohesion, and ii) chemical crosslinking of polysaccharides with multivalent cations, leading to hydrogel structures that trap water within the microstructure. ICP

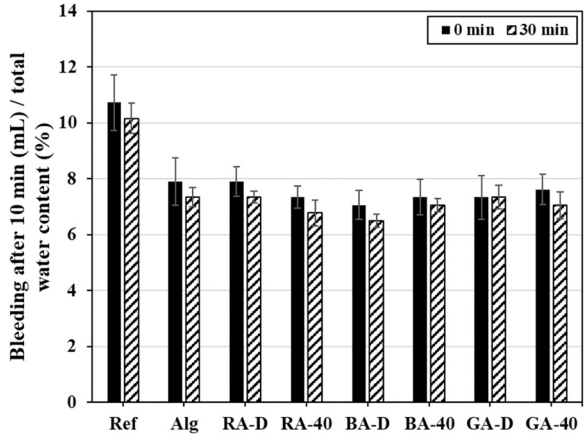

Fig. 10. Forced bleeding of the earth suspensions with and without algae-derived biopolymers at 0 and 30 min.

results support this interpretation, showing that BA systems strongly sequester Ca^{2+}, leading to high free water, which likely contributes to their superior bleeding resistance. When related to rheological measurements, a clear correlation emerges where mixtures with lower bleeding values generally display higher static yield stress and faster structural build-up rates. For instance, BA-D and BA-40, which had the lowest bleeding, also displayed the higher viscosity value (1.00–1.55 Pa.s at 0 min and 28.30–31.90 Pa.s at 30 min) and rigidification rates (≈ 2.0 Pa/s), reflecting the formation of interconnected networks. Overall, the parallel trends observed across bleeding, ICP, and rheology confirm that algae-derived biopolymers improve suspension stability through the synergistic effects of water immobilization and ion crosslinking. Rheological parameters (higher yield stress, faster structural build-up) support the conclusion that algae-derived biopolymers improve fresh-state stability through combined physical immobilization of water and chemical crosslinking with multivalent cations. These mechanisms not only mitigate water migration but may also reduce permeability and promote more uniform hydration in the hardened state, ultimately supporting improved long-term mechanical performance [108].

3.6. Compressive strength and elastic modulus

The compressive strength (f'_c) of the investigated samples at 1, 7, 28, and 56 days is shown in Fig. 11. All biopolymer-modified mixtures exhibited lower 1-day compressive strength ($f'_{c\text{-}1d}$, less than 1 MPa), compared to the reference mixture, reflecting the hydration delays discussed in Section 3.1. The reference mixture showed the earliest first and second hydration peaks (9.1 and 17.9 h) with the highest intensity, consistent with its highest $f'_{c\text{-}1d}$. Among the biopolymer systems, only the alginate-based formulation showed a first peak within 24 h (15.6 and 23.4 h), with a lower initial intensity but a higher second-peak intensity compared to reference, indicating delayed but sustained reactivity. As reported by Murugappan and Muthadhi [117], low alginate dosage (lower than 8 % of cement) can yield compressive strength comparable to reference cement mixture. Alginate enhances mechanical performance primarily via ionic bridging between its polymer chains and divalent Ca^{2+} naturally present in the soil. In aqueous environments, soluble alginate transforms into an insoluble gel through interaction with Ca^{2+}, a process described by the “egg-box model” [43,118]. Here, guluronic acid blocks of negatively charged alginate chains cooperatively coordinate with cations, forming junction zones analogous to eggs in an egg box. Progressive gelation increases chain-to-chain linkages, creating a continuous three-dimensional network that reinforces particle arrangement and water-mediated interactions, which likely explains the mechanical benefits observed in alginate- and BA-modified samples.

At all ages except 1 day, an improvement in compressive strength was observed for the biopolymer-based mixtures. RA-D and BA-D achieved low $f'_{c\text{-}1d}$ of 0.3 and 0.6 MPa, respectively, while the other algae-based mixtures could not be demolded at 24 h and were instead tested at 7 days. These low compressive strength values align with the onset of heat flow observed before the first peak for RA-D and BA-D. Rich in carrageenan, RA-D possess a high sulfate content and strong gelling ability, allowing them to interact electrostatically with Ca^{2+} and Al^{3+} ions, thereby forming compact surface layers on reactive mineral particles [56]. Carrageenan can interact and bind with metal cations. The presence of calcium ions promotes the formation of a threefold, parallel double-helix structure [119]. These calcium ions, together with coordinated water molecules, associate with the peripheral sulfate groups of carrageenan, effectively stabilizing and tightening the helical configuration. As for BA-D, the insoluble fibers, polyphenols, proteins, and minerals in the brown algae matrix delay hydration relative to the reference and alginate samples, but still allow it to occur much sooner than in BA-40 [68]. These changes are driven by ion complexation, surface adsorption, and the increase in mixture viscosity.

At later ages, the compressive strength values of biopolymer-based

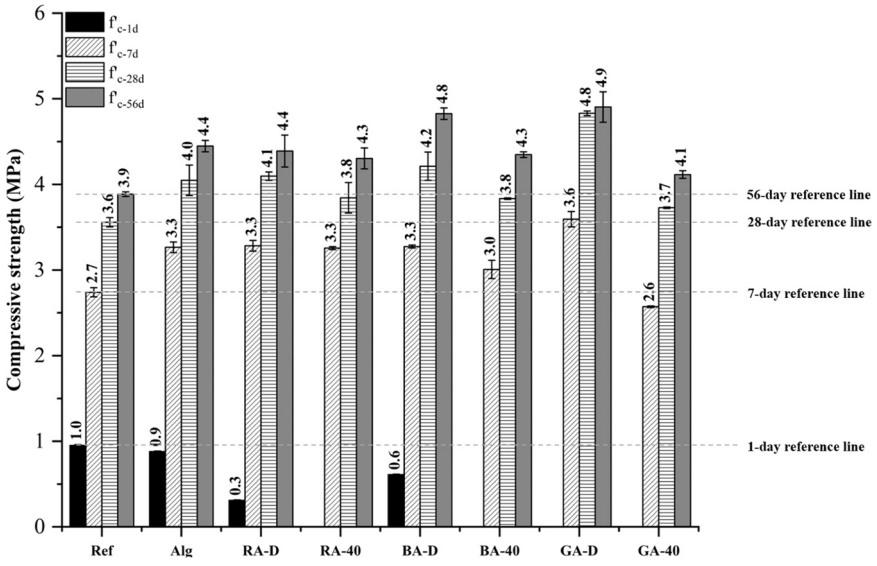

Fig. 11. Compressive strength of the investigated samples.

mixtures surpassed the reference mixture. The only exception is attributed to $f'_{c\text{-}7d}$ of GA-40 which was still slightly less than the reference mixture (2.6 vs. 2.7 MPa). This can be attributed to hydration inhibition, the high PCE dosage required for mixing, and the low saturation point at MSF = 150 mm. These observations align with [17], which reported that excessive high-range water reducer (HRWR) dosage can reduce early-age strength development. Among the other formulations, alginate, RA-D, RA-40, and BA-D exhibited similar $f'_{c\text{-}7d}$ of 3.3 MPa. BA, with its predominant alginate content, and RA, containing κ-carrageenan, achieved comparable results to pure alginate, whereas pre-activated BA was less effective than direct addition with $f'_{c\text{-}7d}$ of 3.0 MPa. Overall, direct addition of the biopolymers consistently resulted in higher compressive at all ages compared to their corresponding pre-activated counterparts, likely due to reduced interference of soluble polysaccharide and other organic components with hydration [56]. Notably, GA-D showed the highest $f'_{c\text{-}7d}$ (3.6 MPa), highlighting the strong efficiency of ulvan in enhancing the mechanical performance of samples.

Ulvan also exhibits a strong capacity to bind with metal ions through covalent interactions, electrostatic forces, or redox reactions. However, its affinity for Ca^{2+} is generally lower than for other cations such as Cr^{3+} or Cu^{2+} [120]. Studies on ion-binding selectivity indicate that ulvan has the highest affinity for Al^{3+}, followed by Cu^{2+}, Pb^{2+}, Zn^{2+}, Cd^{2+}, Mn^{2+}, Sr^{2+}, and Mg^{2+}, with Ca^{2+} showing the weakest binding capacity among the tested ions [121]. This reduced affinity for Ca^{2+} may be attributed to its relatively larger hydrated ionic radius and lower charge density compared to highly charged or more polarizing cations like Al^{3+} or Cr^{3+}, which enables those ions to form stronger and more stable coordination complexes with the functional groups in ulvan, particularly the sulfate and carboxyl moieties. In the context of cementitious systems, this ion-binding profile has important implications. The relatively low interaction between ulvan and Ca^{2+} suggests that the polymer may exert minimal interference with the availability of calcium ions required for the nucleation and growth of calcium silicate hydrate (C-S-H) during early hydration. Conversely, its stronger affinity for multivalent transition metals, such as Al^{3+} and Cu^{2+}, could influence the kinetics of supplementary hydration reactions, alter the incorporation of aluminum into C-S-H, or modify the stability of ettringite and other hydration products. Such selective binding explains the observed effects of GA-D on setting time, microstructure development, and late-age mechanical performance. It should be noted that the cement content used in this study (90 kg/m^3), together with the measured compressive strength, demonstrates that these mixtures represent a viable alternative to traditional earthen construction materials.

3.7. Microstructural observations

SEM observations provide insights into the microstructural organization, the identification of the main hydration products, and the detection of residual mineral phases in both the reference and algae-containing samples (Table 5) [122]. The reference mixture exhibits a compact yet heterogeneous matrix, in which large angular quartz and silt particles are embedded in a continuous C-S-H gel. Well-developed hexagonal portlandite plates are abundant, often located in interstitial spaces or within the interfacial transition zone (ITZ), while elongated ettringite needles tend to form dense clusters. Lamellar particles, attributed to kaolinite, are also visible, consistent with prior observations of kaolinite activation in SCEC [34]. These observations are consistent with the XRD pattern of the reference mixture, confirming kaolinite along with pronounced portlandite and ettringite peaks, indicating the normal progress of cement hydration and the partial dissolution of kaolinite. The ITZ appears irregular and locally porous, consistent with the relatively low 28-day compressive strength (3.6 MPa). In contrast, all algae-based systems display denser and more cohesive matrices than the reference, with a finer C-S-H textures, reduced portlandite crystal size, more dispersed ettringite, and improved ITZ bonding. Lamellar kaolinite particles are more abundant in algae-containing mixtures, in agreement with the XRD patterns. The denser microstructure and improved ITZ may be attributed to the action of polysaccharides in promoting particle cohesion, combined with the contribution of supplementary calcite originating from the algae powders [123]. This calcite could also play a role through filler and nucleation effects, enhancing particle packing within the matrix [124]. These interpretations are supported by the XRD analysis, which shows higher calcite peak intensities in algae-based systems, especially in the case of BA and GA. This improvement in the overall strength and density of the samples incorporating algae-based biopolymers can also be attributed to their high ionic content, as confirmed by the ICP analysis. In particular, the iron oxide (Fe_2O_3) present in the algae may react with calcium from the cement to form calcium alumino-ferrite (C4AF). While this additional hydration phase plays a less prominent role than C-S-H gels, it can still contribute to enhancing the strength and hardness of the matrix. A similar interpretation was reported by Mahamat et al. [125] in a study on Portland cement stabilization of paste specimens with termite hill soil. This mechanism may also explain the higher mechanical strength observed for BA, despite its Ca^{2+} concentration being lower than that of the reference at both 0 and 30 min.

Although both dry and pre-activated algae powders improve matrix

Table 5
SEM images of the investigated samples at 100 and 50 μm.

	100 μm	50 μm
Ref	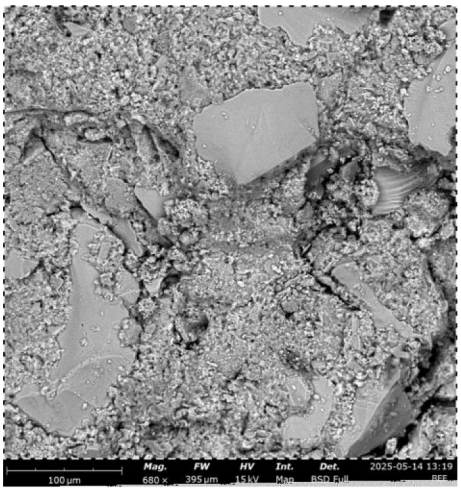	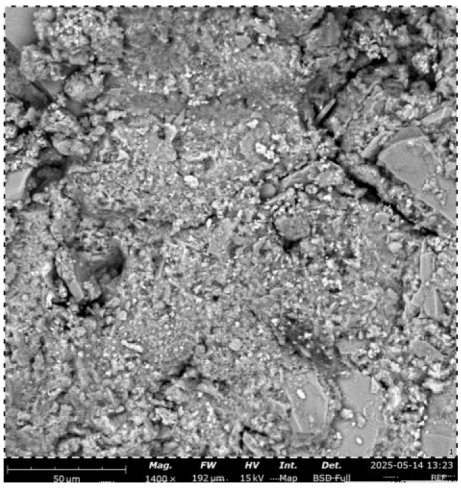
Alg	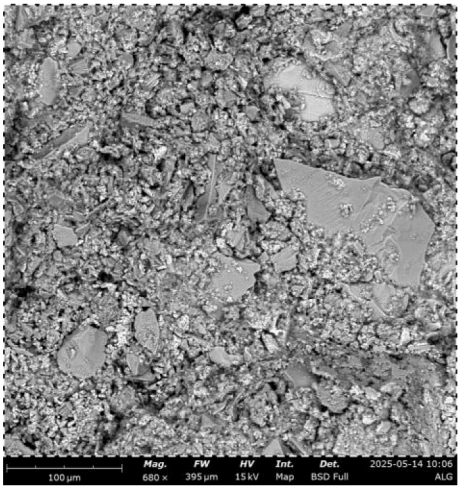	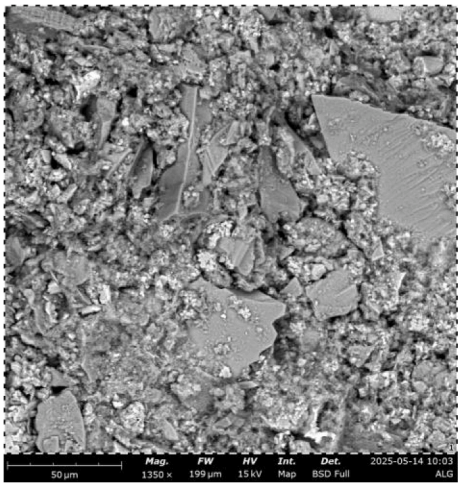
RA-D	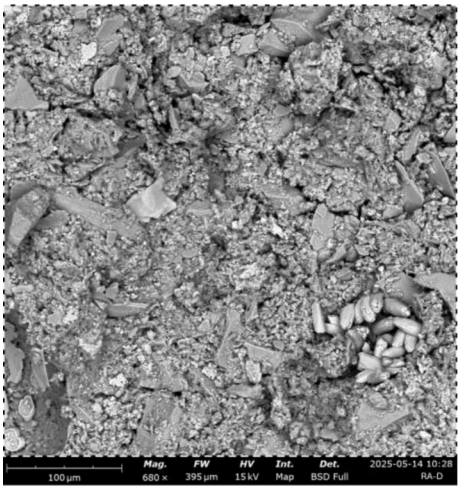	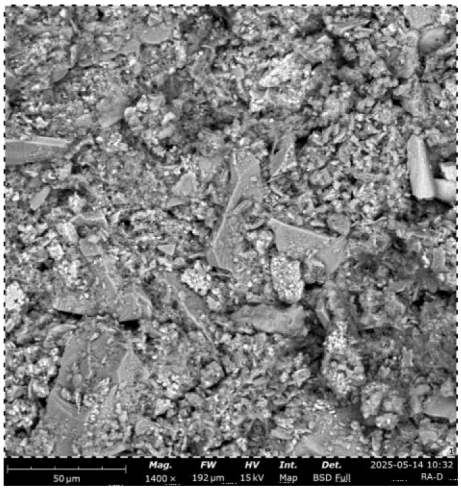

(*continued on next page*)

Table 5 (*continued*)

RA-40	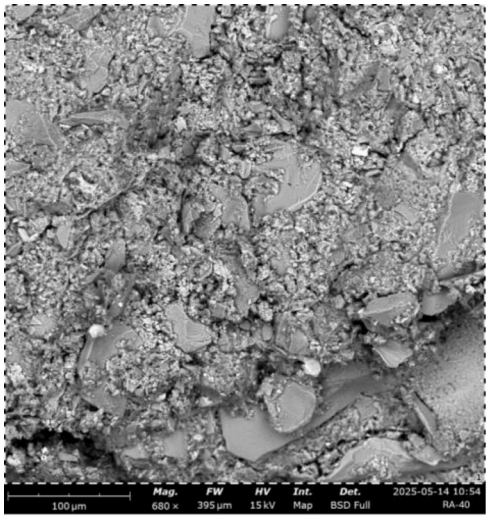	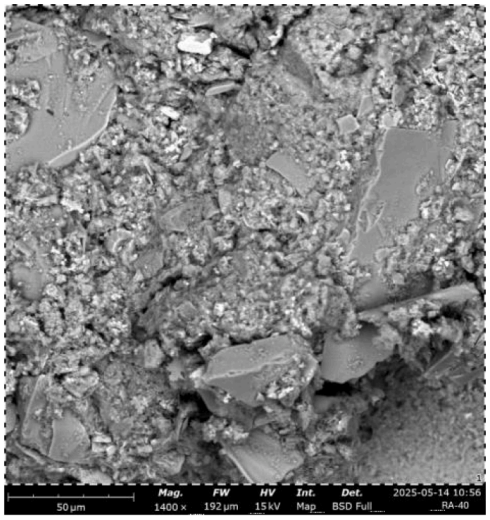
BA-D	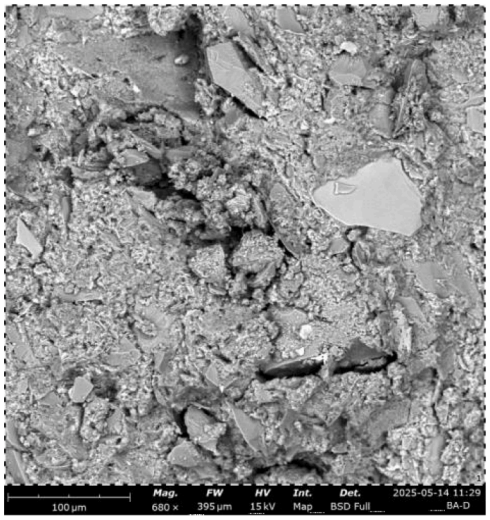	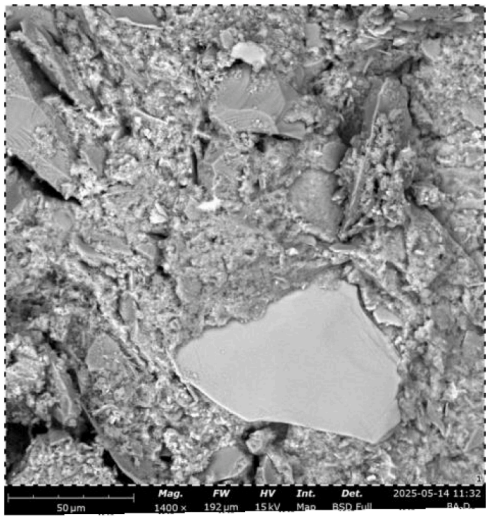
BA-40	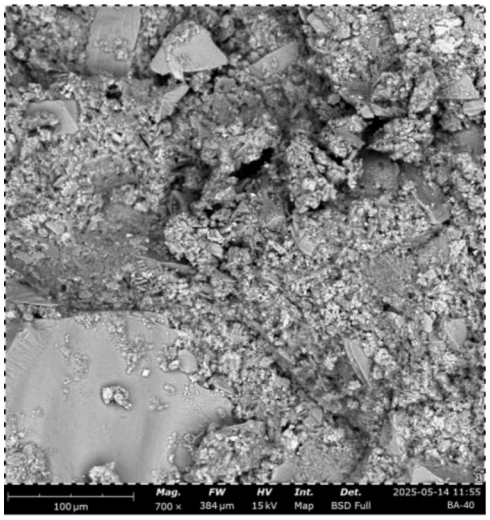	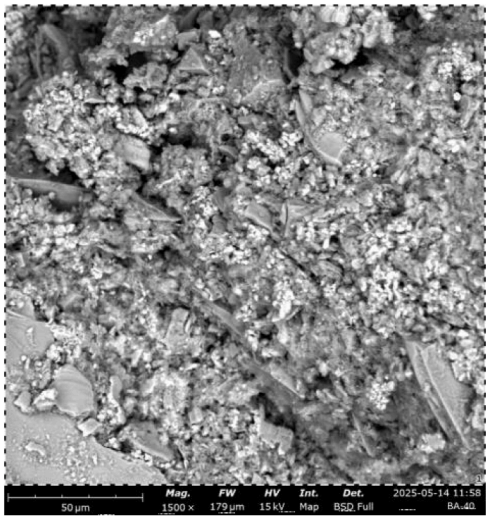

(*continued on next page*)

Table 5 (*continued*)

GA-D	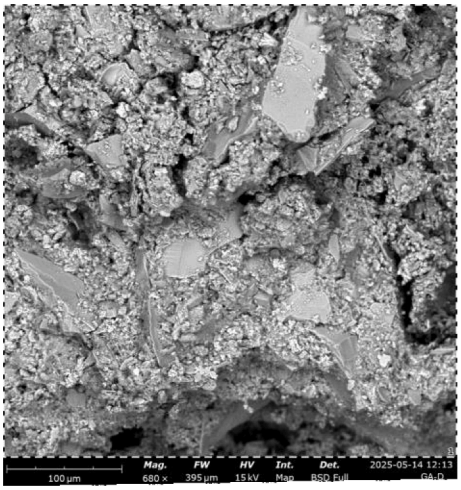	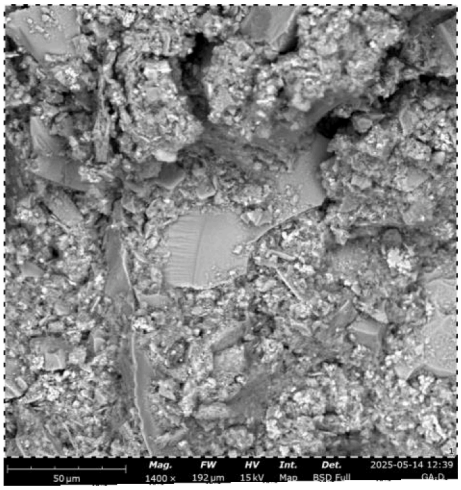
GA-40	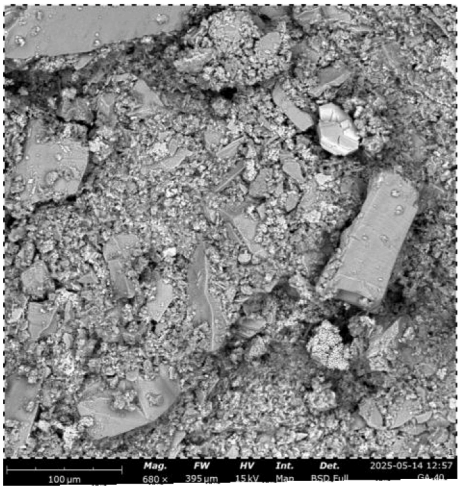	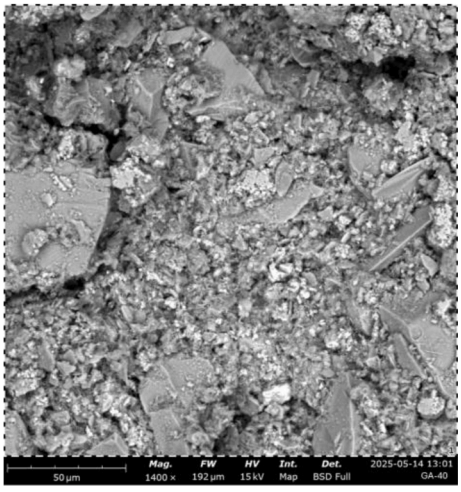

refinement, SEM images suggest that dry systems generally form more homogeneous and better-connected microstructures. This is reflected in the mechanical results, where GA-D achieved the highest compressive strength at 28 days (4.8 MPa), followed by RA-D (4.4 MPa) and BA-D (4.2 MPa). In summary, SEM observations confirm that algae-based biopolymers improve the microstructure compared with the reference by densifying the C-S-H gel, enhancing ITZ quality, reducing portlandite size, and introducing beneficial biogenic calcite.

4. Conclusions

This study demonstrates that algae-derived biopolymers can effectively enhance the performance of cement-stabilized earth concrete, offering a sustainable strategy for low-carbon construction. The key findings and contributions are summarized as follow:

- The effect of algae-based biopolymers strongly depends on botanical origin, biochemical composition, and pre-treatment. Brown algae caused the most pronounced hydration delay, extending the induction period to approximately 88 h, while red and green algae also inhibited early reactions to varying degrees.
- ICP-OES analysis revealed that algae act both as early ion donors and strong chelators of Ca^{2+}, Al^{3+}, and Mg^{2+}, with brown algae showing the highest calcium sequestration. This dual ionic action, combined with biopolymer adhesion to mineral surfaces, explains the observed retardation and highlights the importance of dosage control.
- algae-based biopolymers, as VMAs, improved rheological behavior and fresh-state stability. Brown algae increased plastic viscosity most significantly, whereas green and red algae promoted the formation of a stronger structural network, reducing bleeding and enhancing hydration uniformity.
- Compressive strength development was influenced by biopolymer type. While early-age strength was lower than the reference, directly incorporated green algae achieved the highest 28-day compressive strength (4.8 MPa), demonstrating that biopolymers can enhance long-term mechanical performance.
- SEM analyses indicate that algae-based biopolymers densified the C-S-H gel, refined portlandite crystals, improved the interfacial transition zone, and introduced biogenic calcite, collectively yielding a compact and cohesive microstructure.
- The combination of improved rheology, fresh-state stability, and matrix densification confirms that algae-derived biopolymers are effective eco-efficient admixtures for SCEC, enabling better process control and mechanical performance while maintaining environmental benefits.
- These findings highlight the potential of algae-derived biopolymers to expand the applicability of SCEC in sustainable construction and suggest that further investigation into molecular-scale interactions could optimize formulations for diverse earth-based applications.

CRediT authorship contribution statement

Ammar Yahia: Writing – review & editing, Writing – original draft, Supervision, Resources, Project administration, Formal analysis, Data curation. **Kamal Bouarab:** Writing – review & editing, Supervision, Formal analysis, Data curation. **Mahmoud Hayek:** Writing – review & editing, Writing – original draft, Validation, Software, Methodology, Investigation, Formal analysis, Data curation, Conceptualization. **Mojtaba Kohandelnia:** Writing – review & editing, Writing – original draft, Validation, Software, Methodology, Investigation, Formal analysis, Data curation, Conceptualization.

Declaration of Competing Interest

The authors of the manuscript, entitled "New perspectives into the rheology of earth suspensions modified with algae-derived biopolymers" declare that they have no conflict of interest.

Acknowledgement

The authors wish to thank the financial support of the National Science and Engineering Research Council of Canada (NSERC), PRIMA Quebec, and the industrial partners participating in the NSERC Chair on Development of Flowable Concrete with Adapted Rheology and their Application in Concrete Infrastructures, held by Professor Ammar Yahia at the Université de Sherbrooke.

Data availability

No data was used for the research described in the article.

References

[1] F. Winnefeld, A. Leemann, A. German, B. Lothenbach, CO2 storage in cement and concrete by mineral carbonation, Curr. Opin. Green. Sustain. Chem. 38 (2022) 100672, https://doi.org/10.1016/j.cogsc.2022.100672.
[2] A. Coelho, Preliminary study for self-sufficiency of construction materials in a Portuguese region - Évora, J. Clean. Prod. 112 (2016) 771–786, https://doi.org/10.1016/j.jclepro.2015.06.113.
[3] P. Heidari, P. Rivard, W. Wilson, Multi-objective optimization of cement-based systems containing marine dredged sediment, Constr. Build. Mater. 439 (2024) 137228, https://doi.org/10.1016/j.conbuildmat.2024.137228.
[4] M. Kohandelnia, A. Yahia, From Dry Flowability to Rheology: Advancing Earth-Based Paste Optimization, ACI Mater. J. 122. https://doi.org/10.14359/51749122.
[5] H. Guillaud, H. Houben, Earth Construction: A Comprehensive Guide, Intermediate Technology Publications, 1994.
[6] C.M. Ouellet-Plamondon, G. Habert, Self-compacted clay based concrete (SCCC): Proof-of-concept, J. Clean. Prod. 117 (2016) 160–168, https://doi.org/10.1016/j.jclepro.2015.12.048.
[7] H. Van Damme, H. Houben, Earth concrete. Stabilization revisited, Cem. Concr. Res. 114 (2018) 90–102, https://doi.org/10.1016/J.CEMCONRES.2017.02.035.
[8] R. Bahar, M. Benazzoug, S. Kenai, Performance of compacted cement-stabilised soil, Cem. Concr. Compos 26 (2004) 811–820, https://doi.org/10.1016/j.cemconcomp.2004.01.003.
[9] M. Hall, Y. Djerbib, Rammed earth sample production: context, recommendations and consistency, Constr. Build. Mater. 18 (2004) 281–286, https://doi.org/10.1016/j.conbuildmat.2003.11.001.
[10] M. Kohandelnia, M. Hosseinpoor, A. Yahia, Sustainable Development with Earth Concrete, in: A. Bahrami (Ed.), Adv. Sustain. Concr. Constr, Springer Nature Switzerland, Cham, 2025, pp. 177–200, https://doi.org/10.1007/978-3-031-85052-3_9.
[11] M. Kohandelnia, Development of Self-Consolidating Earth Concrete (SCEC) with Improved Multifunctional Performance for Green Construction, Univ. é De. Sherbrooke (2022). ⟨http://hdl.handle.net/11143/20243⟩.
[12] G. Minke, Building With Earth: Design and Technology of a Sustainable Architecture, BirkhäUse Basel Switz. (2006).
[13] J.C. Morel, A. Mesbah, M. Oggero, P. Walker, means to drastically reduce the environmental impact of construction, Build. Houses Local Mater. 36 (2001) 1119–1126.
[14] D. Ciancio, P. Jaquin, P. Walker, Advances on the assessment of soil suitability for rammed earth, Constr. Build. Mater. 42 (2013) 40–47, https://doi.org/10.1016/j.conbuildmat.2012.12.049.
[15] M. Kohandelnia, M. Hosseinpoor, A. Yahia, R. Belarbi, Multiscale investigation of self-consolidating earthen materials using a novel concrete-equivalent mortar approach, Constr. Build. Mater. 370 (2023) 130700, https://doi.org/10.1016/J.CONBUILDMAT.2023.130700.
[16] M. Kohandelnia, M. Hosseinpoor, A. Yahia, R. Belarbi, Hygrothermal and microstructural characterization of self-consolidating earth concrete (SCEC), J. Build. Eng. 69 (2023) 106287, https://doi.org/10.1016/J.JOBE.2023.106287.
[17] M. Kohandelnia, M. Hosseinpoor, A. Yahia, R. Belarbi, A new approach for proportioning self-consolidating earth paste (SCEP) using the Taguchi method, Constr. Build. Mater. 347 (2022) 128579, https://doi.org/10.1016/J.CONBUILDMAT.2022.128579.
[18] P. Walker, R. Keable, J. Martin, V. Maniatidis, Rammed earth: design and construction guidelines, IHS BRE, 2005.
[19] M. Westerholm, B. Lagerbald, J. Silfwerbrand, E. Forssberg, Influence of fine aggregate characteristics on the rheological properties of mortars, Cem. Concr. Compos 30 (2008) 274–282.
[20] S.K. Ling, A.K.H. Kwan, Adding ground sand to decrease paste volume, increase cohesiveness and improve passing ability of SCC, Constr. Build. Mater. 84 (2015) 46–53.
[21] J.J. Chen, B.H. Li, P.L. Ng, A.K.H. Kwan, Adding granite polishing waste as sand replacement to improve packing density, rheology, strength and impermeability of mortar, Powder Technol. 364 (2020) 404–415.
[22] M. Kohandelnia, M. Hosseinpoor, A. Yahia, R. Belarbi, New insight on rheology of self-consolidating earth concrete (SCEC), Powder Technol. 424 (2023) 118561, https://doi.org/10.1016/J.POWTEC.2023.118561.
[23] S. Guiheneuf, Formul. Et. renforts De. blocs En. Mat. ériau Terre pour une Util. Struct. INSA De. Rennes (2020). ⟨https://tel.archives-ouvertes.fr/tel-03194559⟩.
[24] A.W. Skempton, The Colloidal activity of clays. in: 3rd Int. Conf. Soil Mech. Found. Eng., London, 1953, pp. 47–61.
[25] C. Galán-Marín, C. Rivera-Gómez, J. Petric, Clay-based composite stabilized with natural polymer and fibre, Constr. Build. Mater. 24 (2010) 1462–1468, https://doi.org/10.1016/J.CONBUILDMAT.2010.01.008.
[26] M. Achenza, L. Fenu, On Earth Stabilization with Natural Polymers for Earth Masonry Construction, Mater. Struct. 39 (2006) 21–27.
[27] C.A. Dove, F.F. Bradley, S.V. Patwardhan, Seaweed biopolymers as additives for unfired clay bricks, Mater. Struct. 49 (2016) 4463–4482.
[28] A. Perrot, D. Rangeard, E. Courteille, 3D printing of earth-based materials: processing aspects, Constr. Build. Mater. 172 (2018) 670–676, https://doi.org/10.1016/J.CONBUILDMAT.2018.04.017.
[29] M. Kohandelnia, A. Yahia, Rheology of stabilized earth-based paste, Acids Symp. Publ. 362 (2024) 108–126, https://doi.org/10.14359/51740878.
[30] A.M. Mostafa, A. Yahia, Physico-chemical kinetics of structural build-up of neat cement-based suspensions, Cem. Concr. Res. 97 (2017) 11–27, https://doi.org/10.1016/J.CEMCONRES.2017.03.003.
[31] I. Mehdipour, K.H. Khayat, Understanding the role of particle packing characteristics in rheo-physical properties of cementitious suspensions: A literature review, Constr. Build. Mater. 161 (2018) 340–353, https://doi.org/10.1016/J.CONBUILDMAT.2017.11.147.
[32] G. Landrou, C. Brumaud, F. Winnefeld, R.J. Flatt, G. Habert, Lime as an anti-plasticizer for self-compacting clay concrete, Mater. (Basel) 9 (2016), https://doi.org/10.3390/ma9050330.
[33] B.B. Sabir, S. Wild, J. Bai, Metakaolin and calcined clays as pozzolans for concrete: a review, Cem. Concr. Compos 23 (2001) 441–454, https://doi.org/10.1016/S0958-9465(00)00092-5.
[34] M. Kohandelnia, M. Zerzouri, A. Yahia, K.H. Khayat, Treatment and activation effects on kaolinite-based earth concrete, Constr. Build. Mater. 478 (2025) 141380, https://doi.org/10.1016/j.conbuildmat.2025.141380.
[35] J.V. González-Aviña, M. Hosseinpoor, A. Yahia, M. Kohandelnia, A. Durán-Herrera, Anionic biopolymers to enhance concrete rheological properties for 3D printing applications, J. Build. Eng. (2025) 114493, https://doi.org/10.1016/j.jobe.2025.114493.
[36] P. Brzyski, L. Gazda, Influence of methylcellulose admixture on glauconite clay mortar properties, Constr. Build. Mater. 426 (2024) 136002, https://doi.org/10.1016/j.conbuildmat.2024.136002.
[37] P. Brzyski, Influence of gum arabic admixture on selected properties of clay mortar, Constr. Build. Mater. 451 (2024) 138865, https://doi.org/10.1016/j.conbuildmat.2024.138865.
[38] A.E. Losini, A.C. Grillet, M. Bellotto, M. Woloszyn, G. Dotelli, Natural additives and biopolymers for raw earth construction stabilization – a review, Constr. Build. Mater. 304 (2021) 124507, https://doi.org/10.1016/j.conbuildmat.2021.124507.
[39] Y. Trambitski, O. Kizinievič, F. Gaspar, V. Kizinievič, J.F.A. Valente, Eco-friendly unfired clay materials modified by natural polysaccharides, Constr. Build. Mater. 400 (2023) 132783, https://doi.org/10.1016/j.conbuildmat.2023.132783.
[40] A. Pinel, E. Prud'homme, A. Charlot, E. Fleury, Y. Jorand, Earthen construction: Demonstration of feasibility at 1/2 scale of poured clay concrete construction, Constr. Build. Mater. 312 (2021) 125275, https://doi.org/10.1016/j.conbuildmat.2021.125275.
[41] S. García-Poza, D. Pacheco, J. Cotas, J.C. Marques, L. Pereira, A.M.M. Gonçalves, Marine macroalgae as a feasible and complete resource to address and promote Sustainable Development Goals (SDGs), Integr. Environ. Assess. Manag 18 (2022) 1148–1161, https://doi.org/10.1002/ieam.4598.
[42] S.C. Motshekga, L.T. Temane, J.T. Orasugh, S.S. Ray, Marine Algae and Their Importance BT, in: R. Soni, D.C. Suyal, L. Morales-Oyervides, M. Fouillaud (Eds.), Current Status of Marine Water Microbiology, Springer Nature Singapore, Singapore, 2023, pp. 67–124, https://doi.org/10.1007/978-981-99-5022-5_5.
[43] Y. Autem, N. Bourgougnon, S. Guihéneuf, A. Perrot, Comparative study of effects of various seaweed parietal polysaccharides on rheological, mechanical and

water-durability properties of earth-based materials, Mater. Struct. 56 (2023) 108, https://doi.org/10.1617/s11527-023-02195-9.
[44] A. Boukhatem, K. Bouarab, A. Yahia, Kappaphycus alvarezii Seaweed as Novel Viscosity-Modifying Admixture for Cement-Based Materials, Acids Mater. J. 120 (2023) 15–28, https://doi.org/10.14359/51738805.
[45] ASTM C494, Standard Specification for Chemical Admixtures for Concrete, ASTM Stand. (2017).
[46] ASTM D4318 – 17, Standard Test Methods for Liquid Limit, Plastic Limit, and Plasticity Index of Soils, ASTM Stand. (2017).
[47] ASTM C305-20, Standard Practice for Mechanical Mixing of Hydraulic Cement Pastes and Mortars of Plastic Consistency, ASTM Stand. (2020) 1–3. https://doi.org/10.1520/C0305-20.2.
[48] N. Roussel, C. Stefani, R. Leroy, From mini-cone test to Abrams cone test: measurement of cement-based materials yield stress using slump tests, Cem. Concr. Res. 35 (2005) 817–822, https://doi.org/10.1016/j.cemconres.2004.07.032.
[49] Y. Rifaai, A. Yahia, A. Mostafa, S. Aggoun, E.H. Kadri, Rheology of fly ash-based geopolymer: effect of NaOH concentration, Constr. Build. Mater. 223 (2019) 583–594, https://doi.org/10.1016/J.CONBUILDMAT.2019.07.028.
[50] A. Perrot, D. Rangeard, A. Pierre, Structural built-up of cement-based materials used for 3D-printing extrusion techniques, Mater. Struct. 49 (2016) 1213–1220.
[51] A. Mostafa, A. Yahia, New approach to assess build-up of cement-based suspensions, Cem. Concr. Res. (2016) 174–182, https://doi.org/10.1016/j, cemconres.2016.03.005.
[52] Y. Qian, G. De Schutter, Enhancing thixotropy of fresh cement pastes with nanoclay in presence of polycarboxylate ether superplasticizer (PCE), Cem. Concr. Res. 111 (2018) 15–22, https://doi.org/10.1016/J.CEMCONRES.2018.06.013.
[53] A.M. Mostafa, P. Diederich, A. Yahia, Effectiveness of rotational shear in dispersing concentrated cement suspensions, J. Sustain. Cem. Mater. 4 (2015) 205–214, https://doi.org/10.1080/21650373.2015.1010659.
[54] T. Mezger, Rheol. Handb. users Rotat. Oscil. rheometers Eur. Coat. (2020).
[55] J.V. González-Aviña, M. Hosseinpoor, A. Yahia, A. Durán-Herrera, New biopolymers as viscosity-modifying admixtures to improve the rheological properties of cement-based materials, Cem. Concr. Compos 146 (2024) 105409, https://doi.org/10.1016/J.CEMCONCOMP.2023.105409.
[56] A. Boukhatem, K. Bouarab, A. Yahia, Kappa (κ)-carrageenan as a novel viscosity-modifying admixture for cement-based materials – Effect on rheology, stability, and strength development, Cem. Concr. Compos 124 (2021) 104221, https://doi.org/10.1016/j.cemconcomp.2021.104221.
[57] ASTM C109-20, Standard test method for compressive strength of hydraulic cement mortars (using 2-in. or [50-mm] cube specimens), ASTM Stand. (2020). https://doi.org/10.1520/C0109_C0109M-20B.
[58] S. Rathnarajan, K. Cendrowski, D. Sibera, P. Sikora, Comprehensive evaluation of early-age hydration and compressive strength development in seawater-mixed binary and ternary cementitious systems, Arch. Civ. Mech. Eng. 24 (2024) 1–19, https://doi.org/10.1007/s43452-024-00932-7.
[59] G. Cardinaud, E. Rozière, O. Martinage, A. Loukili, L. Barnes-Davin, M. Paris, D. Deneele, Calcined clay – Limestone cements: Hydration processes with high and low-grade kaolinite clays, Constr. Build. Mater. 277 (2021) 122271, https://doi.org/10.1016/j.conbuildmat.2021.122271.
[60] R. Fernandez, F. Martirena, K.L. Scrivener, The origin of the pozzolanic activity of calcined clay minerals: A comparison between kaolinite, illite and montmorillonite, Cem. Concr. Res. 41 (2011) 113–122, https://doi.org/10.1016/j.cemconres.2010.09.013.
[61] Y. Maierdan, S.J. Armistead, R.A. Mikofsky, Q. Huang, L. Ben-Alon, W.V. Srubar, S. Kawashima, Rheology and 3D printing of alginate bio-stabilized earth concrete, Cem. Concr. Res. 175 (2024) 107380, https://doi.org/10.1016/j.cemconres.2023.107380.
[62] J. Vignesh, B. Ramesh, J.R. Xavier, A review of recent trends in sustainable biopolymer-integrated concrete and its impact on mechanical performance and structural reliability, Int. J. Biol. Macromol. 321 (2025) 146408, https://doi.org/10.1016/J.IJBIOMAC.2025.146408.
[63] Y. Boutouam, M. Hayek, K. Bouarab, A.A. Yahia, C. Rainieri, M. Hayek, K. Bouarab, A.A. Yahia, A Comprehensive review of plant-based biopolymers as viscosity-modifying admixtures in cement-based materials, 2024, Vol. 14, Page 4307 14, Appl. Sci. (2024) 4307, https://doi.org/10.3390/APP14104307.
[64] Y. Li, C. Chen, W. Xia, H. Qiu, Y. Peng, The influence of sodium alginate on kaolinite flocculation in presence of metal ions: Guidance for green processing, Colloids Surf. A Physicochem. Eng. Asp. 707 (2025) 135893, https://doi.org/10.1016/J.COLSURFA.2024.135893.
[65] A. Peschard, A. Govin, J. Pourchez, E. Fredon, L. Bertrand, S. Maximilien, B. Guilhot, Effect of polysaccharides on the hydration of cement suspension, J. Eur. Ceram. Soc. 26 (2006) 1439–1445, https://doi.org/10.1016/j.jeurceramsoc.2005.02.005.
[66] F.R.C. Mo'o, G. Wilar, H.P. Devkota, N. Wathoni, Ulvan, a Polysaccharide from Macroalga Ulva sp.: a review of chemistry, biological activities and potential for food and biomedical applications, Page 5488 10, Appl. Sci. 2020 10 (2020) 5488, https://doi.org/10.3390/APP10165488.
[67] A.A.A. Barros, A. Alves, C. Nunes, M.A. Coimbra, R.A. Pires, R.L. Reis, Carboxymethylation of ulvan and chitosan and their use as polymeric components of bone cements, Acta Biomater. 9 (2013) 9086–9097, https://doi.org/10.1016/J.ACTBIO.2013.06.036.
[68] L. Mazéas, R. Yonamine, T. Barbeyron, B. Henrissat, E. Drula, N. Terrapon, C. Nagasato, C. Hervé, Assembly and synthesis of the extracellular matrix in brown algae, Semin. Cell Dev. Biol. 134 (2023) 112–124, https://doi.org/10.1016/J.SEMCDB.2022.03.005.
[69] B. Johannesson, K. Yamada, L.-O. Nilsson, Y. Hosokawa, Multi-species ionic diffusion in concrete with account to interaction between ions in the pore solution and the cement hydrates, Mater. Struct. 40 (2007) 651–665, https://doi.org/10.1617/s11527-006-9176-y.
[70] L. Zhang, X. Lu, X. Liu, J. Zhou, H. Zhou, Hydration and mobility of interlayer ions of (Nax, Cay)-montmorillonite: a molecular dynamics study, J. Phys. Chem. C. 118 (2014) 29811–29821, https://doi.org/10.1021/jp508427c.
[71] F. Caruso, S. Mantellato, M. Palacios, R.J. Flatt, ICP-OES method for the characterization of cement pore solutions and their modification by polycarboxylate-based superplasticizers, Cem. Concr. Res. 91 (2017) 52–60, https://doi.org/10.1016/J.CEMCONRES.2016.10.007.
[72] B. Lothenbach, F. Winnefeld, Thermodynamic modelling of the hydration of Portland cement, Cem. Concr. Res. 36 (2006) 209–226, https://doi.org/10.1016/J.CEMCONRES.2005.03.001.
[73] K. De Weerdt, M.Ben Haha, G. Le Saout, K.O. Kjellsen, H. Justnes, B. Lothenbach, Hydration mechanisms of ternary Portland cements containing limestone powder and fly ash, Cem. Concr. Res. 41 (2011) 279–291, https://doi.org/10.1016/J.CEMCONRES.2010.11.014.
[74] J.J. Thomas, D. Rothstein, H.M. Jennings, B.J. Christensen, Effect of hydration temperature on the solubility behavior of Ca-, S-, Al-, and Si-bearing solid phases in Portland cement pastes, Cem. Concr. Res. 33 (2003) 2037–2047, https://doi.org/10.1016/S0008-8846(03)00224-2.
[75] F.J. Huertas, L. Chou, R. Wollast, Mechanism of kaolinite dissolution at room temperature and pressure Part II: kinetic study, Geochim. Cosmochim. Acta 63 (1999) 3261–3275, https://doi.org/10.1016/S0016-7037(99)00249-5.
[76] M. Li, L. Pan, J. Li, C. Xiong, Competitive adsorption and interaction between sodium alginate and polycarboxylate superplasticizer in fresh cement paste, Colloids Surf. A Physicochem. Eng. Asp. 586 (2020) 124249, https://doi.org/10.1016/J.COLSURFA.2019.124249.
[77] M. Bilal, T. Rasheed, J.E. Sosa-Hernández, A. Raza, F. Nabeel, H.M.N. Iqbal, Biosorption: An Interplay between Marine Algae and Potentially Toxic Elements—A Review, Page 65 16, Mar. Drugs 2018 16 (2018) 65, https://doi.org/10.3390/MD16020065.
[78] M.F. de Jesus Raposo, A.M.M. Bernardo De Morais, R.M.S. Costa De Morais, Bioactivity and applications of polysaccharides from Marine microalgae, Polysacch. Bioactivity Biotechnol. (2015) 1683–1727, https://doi.org/10.1007/978-3-319-16298-0_47/TABLES/6.
[79] D.B. Stengel, S. Connan, Natural products from marine algae, Fat. Acids Total Lipid Protein Ash Contents Process. Edible Seaweeds 1308 (2015) 103–108. ⟨http://link.springer.com/10.1007/978-1-4939-2684-8⟩ (accessed August 7, 2025).
[80] N. Ahmed, M.A. Sheikh, M. Ubaid, P. Chauhan, K. Kumar, S. Choudhary, Comprehensive exploration of marine algae diversity, bioactive compounds, health benefits, regulatory issues, and food and drug applications, Meas. Food 14 (2024) 100163, https://doi.org/10.1016/J.MEAFOO.2024.100163.
[81] Y. Lu, J. Chen, R. Wang, P. Xu, X. Zhang, B. Gao, C. Guo, G. Yang, Bio-inspired Cu-alginate to smartly enhance safety performance and the thermal decomposition of ammonium perchlorate, Appl. Surf. Sci. 470 (2019) 269–275, https://doi.org/10.1016/J.APSUSC.2018.11.108.
[82] P. Dolmantas, K. Dagilis, A. Jurkevičiūtė, Š. Meškinis, T. Tamulevičius, Al^{3}+ influence on the formation of calcium silicates by using two step synthesis, NBCM 2020 Int. Conf. Nanostruct. Bioceram. Mater. 13 Dec. 2020 Vilnius Vilnius Univ. Conf. Book 28 (2020), 1–1.
[83] C. Hu, W. Lu, A. Mata, K. Nishinari, Y. Fang, Ions-induced gelation of alginate: Mechanisms and applications, Int. J. Biol. Macromol. 177 (2021) 578–588, https://doi.org/10.1016/J.IJBIOMAC.2021.02.086.
[84] F. Yao, M. Li, L. Pan, J. Li, N. Xu, Synthesis of sodium alginate-polycarboxylate superplasticizer and its tolerance mechanism on montmorillonite, Cem. Concr. Compos 133 (2022) 104638, https://doi.org/10.1016/J.CEMCONCOMP.2022.104638.
[85] Y. Wang, C. Yuan, B. Cui, Y. Liu, Influence of cations on texture, compressive elastic modulus, sol-gel transition and freeze-thaw properties of kappa-carrageenan gel, Carbohydr. Polym. 202 (2018) 530–535, https://doi.org/10.1016/J.CARBPOL.2018.08.146.
[86] A. Robic, C. Gaillard, J.F. Sassi, Y. Leral, M. Lahaye, Ultrastructure of Ulvan: A polysaccharide from green seaweeds, Biopolymers 91 (2009) 652–664, https://doi.org/10.1002/BIP.21195;WGROUP:STRING:PUBLICATION.
[87] S.H. Ching, N. Bansal, B. Bhandari, Alginate gel particles–A review of production techniques and physical properties, Crit. Rev. Food Sci. Nutr. 57 (2017) 1133–1152, https://doi.org/10.1080/10408398.2014.965773;SUBPAGE:STRING:FULL.
[88] Q. Fu, Z. Wang, Y. Xue, D. Niu, Catalysis and Regulation of Graphene Oxide on Hydration Properties and Microstructure of Cement-Based Materials, ACS Sustain. Chem. Eng. 11 (2023) 5626–5643, https://doi.org/10.1021/ACSSUSCHEMENG.3C00109/ASSET/IMAGES/LARGE/SC3C00109_0021.JPEG.
[89] E.C. Gaucher, P. Blanc, Cement/clay interactions – A review: Experiments, natural analogues, and modeling, Waste Manag 26 (2006) 776–788, https://doi.org/10.1016/J.WASMAN.2006.01.027.
[90] N. Garg, J. Skibsted, Dissolution kinetics of calcined kaolinite and montmorillonite in alkaline conditions: Evidence for reactive Al(V) sites, J. Am. Ceram. Soc. 102 (2019) 7720–7734, https://doi.org/10.1111/JACE.16663.
[91] N.E. N'Guessan, E. Joussein, A. Courtin-Nomade, E. Paineau, M. Soubrand, O. Grauby, V. Robin, C.D. Cristina, D. Vantelon, P. Launois, P. Fondanèche, S. Rossignol, N. Texier-Mandoki, X. Bourbon, Role of cations on the dissolution

mechanism of kaolinite in high alkaline media, Appl. Clay Sci. 205 (2021) 106037, https://doi.org/10.1016/J.CLAY.2021.106037.
[92] K. Elert, E. Sebastián Pardo, C. Rodriguez-Navarro, Influence of organic matter on the reactivity of clay minerals in highly alkaline environments, Appl. Clay Sci. 111 (2015) 27–36, https://doi.org/10.1016/J.CLAY.2015.03.006.
[93] M.I. Bilan, A.I. Usov, Polysaccharides of Calcareous Algae and Their Effect on the Calcification Process, Russ. J. Bioorg. Chem. 27 (2001) 2–16, https://doi.org/10.1023/A:1009584516443/METRICS.
[94] N. Conci, S. Vargas, G. Wörheide, The Biology and Evolution of Calcite and Aragonite Mineralization in Octocorallia, Front. Ecol. Evol. 9 (2021) 623774, https://doi.org/10.3389/FEVO.2021.623774/XML.
[95] C. Kothari, N. Garg, Quantitative phase analysis of anhydrous Portland cement via combined X-ray diffraction and Raman imaging: Synergy and impact of analysis parameters, Cem. Concr. Res. 186 (2024) 107662, https://doi.org/10.1016/J.CEMCONRES.2024.107662.
[96] P.R. de Matos, J.S. Andrade Neto, D. Jansen, A.G. De la Torre, A.P. Kirchheim, C. E.M. Campos, In-situ laboratory X-ray diffraction applied to assess cement hydration, Cem. Concr. Res. 162 (2022) 106988, https://doi.org/10.1016/J.CEMCONRES.2022.106988.
[97] A. Mignon, D. Snoeck, K. D'Halluin, L. Balcaen, F. Vanhaecke, P. Dubruel, S. Van Vlierberghe, N. De Belie, Alginate biopolymers: Counteracting the impact of superabsorbent polymers on mortar strength, Constr. Build. Mater. 110 (2016) 169–174, https://doi.org/10.1016/j.conbuildmat.2016.02.033.
[98] E. Korda, A. Cousture, E. Tsangouri, D. Snoeck, G. De Schutter, D.G. Aggelis, Active SAP desorption control in concrete through acoustic emission for optimized curing, Cem. Concr. Compos 160 (2025) 106067, https://doi.org/10.1016/j.cemconcomp.2025.106067.
[99] A. Danish, M.A. Mosaberpanah, M.U. Salim, Robust evaluation of superabsorbent polymers as an internal curing agent in cementitious composites, J. Mater. Sci. 56 (2021) 136–172, https://doi.org/10.1007/s10853-020-05131-2.
[100] L.A. dos Santos, Natural Polymeric Biomaterials Processing Properties (2014). ⟨https://api.semanticscholar.org/CorpusID:136389300⟩.
[101] R.M.I.R. Susilorini, H. Hardjasaputra, S. Tudjono, G. Hapsari, S.R. Wahyu, G. Hadikusumo, J. Sucipto, The advantage of natural polymer modified mortar with seaweed: green construction material innovation for sustainable concrete, Procedia Eng. 95 (2014) 419–425.
[102] A. Patti, D. Acierno, H. Lecocq, A. Serghei, P. Cassagnau, Viscoelastic behaviour of highly filled polypropylene with solid and liquid Tin microparticles: influence of the stearic acid additive, Rheol. Acta 60 (2021) 661–673, https://doi.org/10.1007/s00397-021-01297-x.
[103] M.M. Rueda, R. Fulchiron, G. Martin, P. Cassagnau, Linear and non-linear nature of the flow of polypropylene filled with ferrite particles: from low to concentrated composites, Rheol. Acta 56 (2017) 635–648, https://doi.org/10.1007/s00397-017-1025-0.
[104] H.A. Barnes, A review of the rheology of filled viscoelastic systems, Rheol. Rev. (2003) 1–36.
[105] T.F. Tadros, Rheology of dispersions: principles and applications, John Wiley & Sons, 2011.
[106] M. Zhang, J. Liu, Y. Wang, Effects of water hardness on the dispersion of fine coal and kaolinite in coal slurry, Mei T'an Hsueh Pao, J. China Coal Soc. 33 (2008).
[107] K.H. Khayat, Viscosity-enhancing admixtures for cement-based materials — An overview, Cem. Concr. Compos 20 (1998) 171–188, https://doi.org/10.1016/S0958-9465(98)80006-1.
[108] M. Sonebi, A. Perrot, Effect of mix proportions on rheology and permeability of cement grouts containing viscosity modifying admixture, Constr. Build. Mater. 212 (2019) 687–697, https://doi.org/10.1016/J.CONBUILDMAT.2019.04.022.
[109] K.H. Khayat, K.H. Khayat, A. Yahia, Effect of welan gum-high-range water reducer combinations on rheology of cement grout, Artic. Acids Mater. J. 94 (1997). ⟨https://www.researchgate.net/publication/279542729⟩ (accessed August 11, 2025).
[110] J.V. González-Aviña, M. Hosseinpoor, A. Yahia, A. Durán-Herrera, Synergistic effects of superplasticizers and biopolymer-based viscosity-modifying admixtures on the rheology of cement-based systems, Cem. Concr. Compos 154 (2024) 105807, https://doi.org/10.1016/J.CEMCONCOMP.2024.105807.
[111] W. Yin, X. Li, T. Sun, Y. Chen, F. Xu, G. Yan, M. Xu, K. Tian, Utilization of waste glass powder as partial replacement of cement for the cementitious grouts with superplasticizer and viscosity modifying agent binary mixtures: Rheological and mechanical performances, Constr. Build. Mater. 286 (2021) 122953, https://doi.org/10.1016/J.CONBUILDMAT.2021.122953.
[112] M. Hayek, Y. El Bitouri, K. Bouarab, A. Yahia, Structural Build-Up of Cement Pastes: A Comprehensive Overview and Key Research Directions, Page 31 5, Constr. Mater. 2025 5 (2025) 31, https://doi.org/10.3390/CONSTRMATER5020031.
[113] J. Wang, A. Mignon, D. Snoeck, V. Wiktor, S. Van Vliergerghe, N. Boon, N. De Belie, Application of modified-alginate encapsulated carbonate producing bacteria in concrete: A promising strategy for crack self-healing, Front. Microbiol 6 (2015) 161155, https://doi.org/10.3389/FMICB.2015.01088/BIBTEX.
[114] T. Žižlavský, P. Bayer, M. Vyšvařil, Bond Properties of NHL-Based Mortars with Viscosity-Modifying Water-Retentive Admixtures, Page 685 11, Miner 2021 11 (2021) 685, https://doi.org/10.3390/MIN11070685.
[115] G. Jose, K.T. Shalumon, J.-P. Chen, Natural Polymers Based Hydrogels for Cell Culture Applications, Curr. Med. Chem. 27 (2019) 2734–2776, https://doi.org/10.2174/0929867326666190903113004.
[116] L. Krishnan, N. Ravi, A. Kumar Mondal, F. Akter, M. Kumar, P. Ralph, U. Kuzhiumparambil, Seaweed-based polysaccharides – review of extraction, characterization, and bioplastic application, Green. Chem. 26 (2024) 5790–5823, https://doi.org/10.1039/D3GC04009G.
[117] V. Murugappan, A. Muthadhi, Studies on the influence of alginate as a natural polymer in mechanical and long-lasting properties of concrete – A review, Mater. Today Proc. 65 (2022) 839–845, https://doi.org/10.1016/j.matpr.2022.03.424.
[118] C. Dove, The development of unfired earth bricks using seaweed biopolymers, WIT Trans. Built Env. 142 (2014) 219–230.
[119] S. Janaswamy, R. Chandrasekaran, Effect of calcium ions on the organization of iota-carrageenan helices: an X-ray investigation, Carbohydr. Res. 337 (2002) 523–535, https://doi.org/10.1016/S0008-6215(02)00017-4.
[120] Y. Chi, H. Li, L. Fan, C. Du, J. Zhang, H. Guan, P. Wang, R. Li, Metal-ion-binding properties of ulvan extracted from Ulva clathrata and structural characterization of its complexes, Carbohydr. Polym. 272 (2021) 118508, https://doi.org/10.1016/j.carbpol.2021.118508.
[121] A. Alves, R.A. Sousa, R.L. Reis, A practical perspective on ulvan extracted from green algae, J. Appl. Phycol. 25 (2013) 407–424, https://doi.org/10.1007/s10811-012-9875-4.
[122] P. Li, W. Li, K. Wang, H. Zhao, S.P. Shah, Hydration and microstructure of cement paste mixed with seawater – An advanced investigation by SEM-EDS method, Constr. Build. Mater. 392 (2023) 131925, https://doi.org/10.1016/J.CONBUILDMAT.2023.131925.
[123] R. Pei, J. Liu, S. Wang, M. Yang, Use of bacterial cell walls to improve the mechanical performance of concrete, Cem. Concr. Compos 39 (2013) 122–130, https://doi.org/10.1016/J.CEMCONCOMP.2013.03.024.
[124] E. Berodier, K. Scrivener, Understanding the Filler Effect on the Nucleation and Growth of C-S-H, J. Am. Ceram. Soc. 97 (2014) 3764–3773, https://doi.org/10.1111/JACE.13177.
[125] A.A. Mahamat, N. Leklou, Ifeyinwa, I. Obianyo, Tido, T. Stanislas, O. Ayeni, Numfor, L. Bih, Evaluation of the microstructural and physico-mechanical characteristics of cement-stabilized termite hill soil for construction application, Discov. Civ. Eng. 2024 (11 1) (2024) 1–15, https://doi.org/10.1007/S44290-024-00058-Y.